

## Conjugate comparison of Super Dual Auroral Radar Network and Cluster electron drift instrument measurements of $\mathbf{E} \times \mathbf{B}$ plasma drift

J. B. H. Baker,<sup>1</sup> R. A. Greenwald,<sup>1</sup> J. M. Ruohoniemi,<sup>1</sup> M. Förster,<sup>2</sup> G. Paschmann,<sup>2</sup>  
E. F. Donovan,<sup>3</sup> N. A. Tsyganenko,<sup>4</sup> J. M. Quinn,<sup>5</sup> and A. Balogh<sup>6</sup>

Received 25 February 2003; revised 7 August 2003; accepted 25 August 2003; published 17 January 2004.

[1] Much of our current understanding of magnetospheric electrodynamics is based on the assumption that magnetic field lines often behave as electrostatic equipotentials. This assumption has allowed hemispheric patterns of ionospheric convection to be interpreted in terms of the large-scale circulation of plasma in the magnetosphere. However, the extent to which the equipotential field-line assumption is justified for different regions of the magnetosphere has not been adequately explored, largely because of the sparseness of magnetospheric measurements. In this paper, a mathematical formalism is developed that allows conjugate magnetospheric and ionospheric measurements to be compared with each other using a model magnetic field. The technique is demonstrated during an event interval in which Super Dual Auroral Radar Network measurements of ionospheric plasma drift are mapped to the magnetosphere using the Tsyganenko T01 magnetic field model and compared with conjugate measurements from the Cluster spacecraft electron drift instrument. The degree of consistency between the conjugate measurements is discussed in terms of (1) the accuracy of the magnetic field model, (2) the validity of the assumption of equipotential magnetic field lines, and (3) the presence of inductive electric fields in the magnetosphere. It is also shown how conjugate plasma drift measurements can be used to identify small inaccuracies in the location of ionospheric foot points specified by the magnetic model.

*INDEX TERMS:* 2431 Ionosphere: Ionosphere/magnetosphere interactions (2736); 2463 Ionosphere: Plasma convection; 2494 Ionosphere: Instruments and techniques; 2760 Magnetospheric Physics: Plasma convection; *KEYWORDS:* Tsyganenko, field-aligned potential, inductive electric field, electrostatic mapping

**Citation:** Baker, J. B. H., R. A. Greenwald, J. M. Ruohoniemi, M. Förster, G. Paschmann, E. F. Donovan, N. A. Tsyganenko, J. M. Quinn, and A. Balogh (2004), Conjugate comparison of Super Dual Auroral Radar Network and Cluster electron drift instrument measurements of  $\mathbf{E} \times \mathbf{B}$  plasma drift, *J. Geophys. Res.*, 109, A01209, doi:10.1029/2003JA009912.

### 1. Introduction

[2] Since the beginnings of magnetospheric science, it has been recognized that the high-latitude ionosphere can be used to image electrodynamic processes occurring in the Earth's magnetosphere. The earliest theories of the solar wind-magnetosphere interaction were formulated from patterns of equivalent ionospheric currents that were interpreted in terms of the circulation of magnetospheric plasma driven by the solar wind [Axford and Hines, 1961] and the interplanetary magnetic field (IMF) [Dungey, 1961]. Later, Boström

[1967] made inferences about the properties of magnetospheric electric fields based on observations of visible aurora and ionospheric electric fields. In more recent years, there have been opportunities to deploy instruments on spacecraft for in situ measurements of magnetospheric electric fields and plasma convection [e.g., Pedersen *et al.*, 1984; Baumjohann and Haerendel, 1985]. However, it has been difficult to observe the coherent large-scale dynamics of magnetospheric convection on the temporal and spatial scales required to understand most magnetospheric processes. Thus even to this day, our ability to study global magnetospheric electrodynamics is still based largely on measurements obtained within the Earth's ionosphere. Specific examples include routine measurements of the maximum electrostatic potential difference across the polar cap (the so-called "cross-polar potential") [e.g., Reiff and Luhmann, 1986; Eriksson *et al.*, 2000; Ruohoniemi *et al.*, 2001; Shepherd *et al.*, 2002] and the determination of IMF-dependent patterns of ionospheric convection [e.g., Heppner and Maynard, 1987; Weimer, 1995; Ruohoniemi and Greenwald, 1996].

[3] The early works of Axford and Hines [1961] and Dungey [1961] were based on qualitative mappings of ionospheric convection to the outer magnetosphere. More

<sup>1</sup>Applied Physics Laboratory, Johns Hopkins University, Laurel, Maryland, USA.

<sup>2</sup>Max-Planck-Institut für Extraterrestrische Physik, Garching, Germany.

<sup>3</sup>Department of Physics and Astronomy, University of Calgary, Calgary, Alberta, Canada.

<sup>4</sup>Universities Space Research Association and NASA Goddard Space Flight Center, Greenbelt, Maryland, USA.

<sup>5</sup>Department of Physics, University of New Hampshire, Durham, New Hampshire, USA.

<sup>6</sup>Physics Department, Imperial College, London, UK.

recent studies have used empirical magnetic field models, and the assumption of equipotential magnetic field lines, to do the mapping in a more rigorous fashion. For example, *Donovan and Rostoker* [1991] projected IMF-dependent Heppner-Maynard [*Heppner and Maynard*, 1987] patterns to the equatorial plane using the Tsyganenko T87 and T89 magnetic field models [*Tsyganenko*, 1987, 1989] and compared the results with in situ measurements from the ISEE 1 spacecraft. In a similar manner, *Doe et al.* [1992] combined the equatorial projection of the low-latitude portion of Heppner-Maynard patterns with a corotation electric potential and interpreted the resulting patterns in terms of IMF-dependent behavior of the plasmasphere. Likewise, *Maynard et al.* [1995] examined equatorial projections of Heppner-Maynard patterns and concluded that an apparent mismatch between the local-time features of ionospheric convection and cusp precipitation could be attributed to corotation. More recently, ground- and satellite-based ionospheric data sets have been combined using the assimilative mapping of ionospheric electrodynamics (AMIE) technique [*Richmond and Kamide*, 1988] and projected to the equatorial magnetosphere for analysis during substorms [*Lu et al.*, 2000] and storms [*Boonsirisetth et al.*, 2001].

[4] A theoretical treatment by *Hesse et al.* [1997] investigated the accuracy of using ionospheric measurements to predict electric fields and plasma convection in the magnetosphere. They showed that for time-stationary magnetic fields and no dissipation (i.e., ideal magnetohydrodynamic (MHD)), the electric field at any location is given by the gradient of an electrostatic potential that is constant along magnetic field lines. Under these circumstances, it is perfectly appropriate to infer the magnetospheric electric field from ionospheric measurements. However, if the magnetic field varies with time, then the electric field has an additional inductive component that does not map along magnetic field lines to the ionosphere, and therefore drives a component of magnetospheric convection that cannot be determined from ionospheric measurements. *Hesse et al.* [1997] also investigated the effect of a magnetic-field-aligned electric potential difference on the mapping of convection between the ionosphere and magnetosphere. They determined that these so-called “parallel electric fields” produce a distortion to the mapped convection that is dependent on the gradient in parallel potential difference perpendicular to the magnetic field, rather than the magnitude of the parallel potential difference itself. This means that parallel potential differences of only a few kilovolts can be associated with significant distortions in the convection, provided that the foot points of the parallel electric fields are sufficiently localized in the ionosphere. Observations indicate that parallel electric fields are actually quite common in the auroral zone [e.g., *Evans*, 1974; *Block*, 1988; *Fung and Hoffman*, 1991; *Mozer and Kletzing*, 1998].

[5] Rigorous analysis of the extent to which convection in the magnetosphere and ionosphere is coupled requires a systematic comparison of conjugate electric fields throughout the magnetosphere-ionosphere system under varying geomagnetic conditions. Ideally, the two sets of measurements should have significant contact time so that

the spatial and temporal variability of the two time series can be better evaluated. Such an undertaking has been difficult before now because of the sparseness of simultaneously available conjugate measurements. However, the recent growth of the Super Dual Auroral Radar Network (SuperDARN) provides new opportunities for this type of comparison. The SuperDARN radars operate continuously, providing extensive measurements of drift velocities in regions where ionospheric irregularities produce measurable backscatter within the radar field of view [*Greenwald et al.*, 1985]. The combined fields of view of the SuperDARN radars are now large enough to monitor convection at the ionospheric foot point of a magnetospheric spacecraft during a significant fraction of a pass over the polar region. The European Space Agency (ESA) Cluster mission [*Escoubet et al.*, 2001] includes two electric field experiments that are suitable for conjugate comparison with SuperDARN. The electric field and waves (EFW) instrument utilizes spherical probes at the end of long booms to measure the component of the electric field that lies in the spin plane of the spacecraft [*Gustafsson et al.*, 1997]. The electron drift instrument (EDI) measures the electric field by tracking the guiding center drift of an electron beam injected perpendicular to the magnetic field [*Paschmann et al.*, 1997]. We have chosen to use EDI measurements in this paper because EDI provides a three-component measurement of the plasma drift, making it ideal for conjugate comparison with SuperDARN.

[6] The first objective of the paper is to present a mathematical formalism that allows comparison of simultaneous conjugate magnetospheric and ionospheric measurements of  $\mathbf{E} \times \mathbf{B}$  convection using a model magnetic field. We then present one case study event in which SuperDARN measurements are mapped to the magnetosphere using the Tsyganenko T01 magnetic model [*Tsyganenko*, 2002a, 2002b] and compared with EDI measurements from one of the Cluster spacecraft. The particular event was selected because of the availability of simultaneous conjugate measurements for an extended period of time during a Northern Hemisphere pass of the Cluster spacecraft. The overall trends in the EDI and SuperDARN measurements during the event are largely consistent with each other, but there are significant inconsistencies. The second objective of the paper is to evaluate the inconsistencies in terms of the following sources: (1) the accuracy of the T01 magnetic field model; (2) the validity of the assumption of electrostatic equipotential magnetic field lines; and (3) the presence of inductive electric fields in the magnetosphere. Four sub-event intervals labeled A–D are selected for detailed study because they contain significant EDI-SuperDARN inconsistencies. It is also shown how small inaccuracies in the ionospheric foot point locations specified by the T01 model can sometimes be identified and reduced. Since the primary aim of the paper is to introduce a methodology that will be used in future papers, for simplicity, we focus the analysis on EDI measurements from the Cluster-3 spacecraft only. However, when appropriate, the extent to which the Cluster-3 measurements are consistent with the other Cluster spacecraft is discussed in the text. A more detailed analysis of conjugate

convection using the full multipoint capabilities of the Cluster mission is deferred to future efforts.

## 2. Electrostatic Mapping of Plasma Convection Along Equipotential Magnetic Fields

[7] In this section, we present a general mathematical formalism that will be used to compare electrostatic fields and plasma drifts between two locally small regions that are connected by magnetic field lines assumed to be electric equipotentials. This formalism is then extended to a comparison of drift velocity measurements obtained from a magnetospheric spacecraft with conjugate measurements at the magnetic foot point in the ionosphere. Unless otherwise stated, we assume GSM coordinates throughout this section and the rest of the paper.

### 2.1. Mathematical Formalism

[8] We consider two points,  $\mathbf{P}_0$  and  $\mathbf{P}'_0$ , connected by a magnetic field line,  $L_0$ . We assume mutual orthogonality between the directions of the electric field, the magnetic field, and the plasma drift velocity at both points. In this case, the electric fields at  $\mathbf{P}_0$  and  $\mathbf{P}'_0$  are

$$\mathbf{E}_0 = -\mathbf{V}_0 \times \mathbf{B}_0, \quad (1a)$$

$$\mathbf{E}'_0 = -\mathbf{V}'_0 \times \mathbf{B}'_0, \quad (1b)$$

where  $\mathbf{B}_0$  and  $\mathbf{B}'_0$  are the respective magnetic fields at the endpoints  $\mathbf{P}_0$  and  $\mathbf{P}'_0$ , while  $\mathbf{V}_0$  and  $\mathbf{V}'_0$  are the corresponding plasma drift velocities. We seek an expression that relates  $\mathbf{V}_0$  and  $\mathbf{V}'_0$ . To that end, we consider two additional points:

$$\mathbf{P}_1 = \mathbf{P}_0 + \mathbf{dr}_1, \quad (2a)$$

$$\mathbf{P}'_1 = \mathbf{P}'_0 + \mathbf{dr}'_1, \quad (2b)$$

where  $\mathbf{dr}_1$  and  $\mathbf{dr}'_1$  are two small vectors, such that  $\mathbf{P}_1$  and  $\mathbf{P}'_1$  are connected by a second magnetic field line  $L_1$ . We make the following assumptions: (1) the situation is electrostatic; (2) the magnetic field lines  $L_0$  and  $L_1$  are electric equipotentials; and (3) the vectors  $\mathbf{dr}_1$  and  $\mathbf{dr}'_1$  are both sufficiently small that the electric field does not change along their lengths (i.e.,  $\mathbf{E}_1 = \mathbf{E}_0$  and  $\mathbf{E}'_1 = \mathbf{E}'_0$ ). In this case, the difference in electrostatic potential at the endpoints of  $L_0$  and  $L_1$  are given by the following equivalent relations:

$$\Delta\Phi = \mathbf{E}_0 \cdot \mathbf{dr}_1, \quad (3a)$$

$$\Delta\Phi' = \mathbf{E}'_0 \cdot \mathbf{dr}'_1. \quad (3b)$$

[9] These expressions can be equated and rearranged using equation (1) to obtain

$$(\mathbf{dr}'_1 \times \mathbf{B}'_0) \cdot \mathbf{V}'_0 = (\mathbf{dr}_1 \times \mathbf{B}_0) \cdot \mathbf{V}_0. \quad (4)$$

Equation (4) provides a single constraint on the relationship between the drift velocities at the endpoints of the magnetic field lines in terms of the magnetic field vectors and the spacing between the magnetic field lines. In order to obtain a fully constrained relationship it is necessary to consider

one additional magnetic field line,  $L_2$ , whose starting point is separated from the point  $\mathbf{P}_0$  by the small vector  $\mathbf{dr}_2$  and whose endpoint is separated from  $\mathbf{P}'_0$  by  $\mathbf{dr}'_2$ . Adopting the same assumptions for the additional magnetic field line we can specify the following system of three equations:

$$(\mathbf{dr}'_1 \times \mathbf{B}'_0) \cdot \mathbf{V}'_0 = (\mathbf{dr}_1 \times \mathbf{B}_0) \cdot \mathbf{V}_0, \quad (5a)$$

$$(\mathbf{dr}'_2 \times \mathbf{B}'_0) \cdot \mathbf{V}'_0 = (\mathbf{dr}_2 \times \mathbf{B}_0) \cdot \mathbf{V}_0, \quad (5b)$$

$$0 = \mathbf{B}_0 \cdot \mathbf{V}_0, \quad (5c)$$

where equation (5c) simply imposes our initial assumption that the drift velocity is perpendicular to the magnetic field direction. The relationship between  $\mathbf{V}_0$  and  $\mathbf{V}'_0$  is now fully constrained in terms of the magnetic field vectors and the three-dimensional spacing between the magnetic field lines in the vicinities of  $\mathbf{P}_0$  and  $\mathbf{P}'_0$ . If a suitable method exists for mapping magnetic field lines between two regions, then equations (5a)–(5c) can be solved simultaneously for an unknown drift velocity in one location, if the drift velocity is specified at the other location.

### 2.2. Magnetosphere-Ionosphere Mapping

[10] As an example, we consider the specific case of a single spacecraft at point  $\mathbf{P}_0$  in the magnetosphere taking measurements of the plasma drift velocity,  $\mathbf{V}_0$ . We specify the starting points of a bundle of three magnetic field lines in the vicinity of the spacecraft, one of which,  $L_0$ , intersects the spacecraft location at  $\mathbf{P}_0$  and intersects the ionosphere at  $\mathbf{P}'_0$ . We use a magnetic field model to identify  $\mathbf{P}'_0$  and the ionospheric foot point locations of the other two magnetic field lines  $L_1$  and  $L_2$ . If the ionospheric convection velocity,  $\mathbf{V}'_0$ , is available from ionospheric measurements, then equations (5a)–(5c) can be solved simultaneously for the magnetospheric velocity,  $\mathbf{V}_0$ . However, ionospheric measurements are most commonly obtained with respect to the rotating Earth, whereas spacecraft measurements are usually expressed in Sun-fixed coordinates. The ionospheric measurements therefore need to be converted to Sun-fixed coordinates by adding a corotation velocity given by

$$\mathbf{V}_{\text{rot}} = \omega(R_E + h) \cos \Lambda \hat{\varphi}, \quad (6)$$

where  $\omega$  is the angular frequency of the Earth's rotation,  $R_E$  is the radius of the Earth,  $h$  is the altitude at  $\mathbf{P}'_0$ ,  $\Lambda$  is the geographic latitude, and  $\hat{\varphi}$  is the unit vector in the eastward direction. In the electrostatic case, the ionospheric electric field can be expressed in terms of an electrostatic potential,  $\Phi'$ , and equations (5a)–(5c) can be rewritten in the form:

$$\Phi'_1 - \Phi'_0 = -(\mathbf{dr}_1 \times \mathbf{B}_0) \cdot \mathbf{V}_0, \quad (7a)$$

$$\Phi'_2 - \Phi'_0 = -(\mathbf{dr}_2 \times \mathbf{B}_0) \cdot \mathbf{V}_0, \quad (7b)$$

$$0 = \mathbf{B}_0 \cdot \mathbf{V}_0, \quad (7c)$$

where  $\Phi'_i$  is the electrostatic potential in Sun-fixed coordinates at the ionospheric foot point of field line  $L_i$ . In practice, we have the freedom to choose the vectors  $\mathbf{dr}_1$

and  $\mathbf{dr}_2$  arbitrarily, so long as they are not along the direction of the primary magnetic field line,  $L_0$ . A simple choice is to specify that  $\mathbf{dr}_1$  and  $\mathbf{dr}_2$  are of equal length,  $\Delta l$ , and aligned, respectively, along the directions of the GSM  $x$  and  $y$  axes (provided that  $\mathbf{B}_0$  does not lie in the  $x$ - $y$  plane). In this case, equations (7a)–(7c) can be expressed as

$$\Phi'_1 - \Phi'_0 = \Delta l (B_{0z} V_{0y} - B_{0y} V_{0z}), \quad (8a)$$

$$\Phi'_2 - \Phi'_0 = \Delta l (-B_{0z} V_{0x} - B_{0x} V_{0z}), \quad (8b)$$

$$0 = B_{0x} V_{0x} + B_{0y} V_{0y} + B_{0z} V_{0z}, \quad (8c)$$

where  $\mathbf{V}_0 = (V_{0x}, V_{0y}, V_{0z})$  and  $\mathbf{B}_0 = (B_{0x}, B_{0y}, B_{0z})$ . In this form, equations (8a)–(8c) relate the distribution of electrostatic potential in the vicinity of the ionospheric foot point of a magnetospheric spacecraft (left-hand sides) to the magnetic field and drift velocity at the spacecraft location (right-hand sides). Using ionospheric measurements and a magnetic field model it is possible to solve equations (8a)–(8c) simultaneously for an estimate of the magnetospheric plasma drift velocity,  $\mathbf{V}_0$ , which can then be compared with the spacecraft measurements. If magnetic measurements are available at the spacecraft then they can be used in equations (8a)–(8c) instead of the model magnetic values, in which case, the role of the magnetic model is confined to defining the magnetic conjugacy between the spacecraft and the ionosphere.

[11] These equations provide a useful framework with which to evaluate the consistency between ionospheric and magnetospheric measurements in terms of our understanding of magnetosphere-ionosphere coupling. A number of factors might contribute to apparent inconsistencies between the ionospheric and magnetospheric measurements. Examples of geophysical influences that might violate the initial assumptions used to derive the equations include (1) spatial gradients in the magnetic field across the field line bundle, (2) spatial gradients in the perpendicular electric field across the bundle, (3) the presence of inductive electric fields, and (4) perpendicular gradients in parallel electric field across the bundle. It should be emphasized that in the last case, the presence of a parallel electric field, in and of itself, is not sufficient to explain any inconsistencies if the parallel electric field is constant across the whole ionosphere. Rather, it is a “perpendicular gradient” in parallel electric field that produces partial decoupled convection between the magnetosphere and the ionosphere [Hesse *et al.*, 1997]. Other inconsistencies might be associated with the accuracy of the magnetic field model and the specification of magnetic foot points in the ionosphere. In section 4.2 we demonstrate how one can identify suitable error estimates for the location of the T01 foot points. Section 4.5 introduces a method that seeks to minimize the error in the foot point locations.

[12] In most cases, rigorous identification of a particular inconsistency with a single source or collection of sources can be difficult. For example, localized parallel electric fields may, in some cases, be associated with the presence of field-aligned currents that alter the mapping of magnetic field lines between the magnetosphere and the ionosphere.

However, it is sometimes possible to use contextual information from other measurements to arrive at some qualitative conclusions as to which sources of inconsistency might be dominant in some situations. This will be demonstrated for the case study analysis in section 4.

### 3. Data Sets and Models

[13] In this section, the Tsyganenko T01 magnetic field model is introduced, and the characteristics of the Cluster EDI and SuperDARN instrumentation are described.

#### 3.1. Tsyganenko T01 Magnetic Field Model

[14] The Tsyganenko magnetic field models specify external contributions to the magnetospheric magnetic field through a combination of mathematical formalism and empirical modeling [e.g., Tsyganenko, 1987, 1989, 1995, 2002a, 2002b]. The most recent of these (hereafter “T01”) [Tsyganenko, 2002a, 2002b] is represented as the sum of magnetic effects from up to five current systems: (1) the Chapman-Ferraro currents on the magnetopause; (2) the ring current; (3) the cross-tail current; (4) the large-scale field-aligned currents (regions 1 and 2); and (5) shielding currents to ensure that the magnetic effects are wholly contained within the magnetopause. There is also an additional contribution associated with partial penetration of the IMF into the dayside magnetosphere. The magnetopause size and shape are specified by the solar wind dynamic pressure and dipole tilt angle [Shue *et al.*, 1998]. The T01 model incorporates several improvements over its predecessors. It is better constrained by in situ observations, has a more sophisticated mathematical specification of the currents, an improved fitting procedure, and more realistic parameterization on solar wind and IMF. The total field includes 24 coefficients and 18 nonlinear parameters determined by optimal fitting of magnetometer data from seven spacecraft missions spanning 1984–1999. The input parameters to the T01 model are solar wind dynamic pressure, IMF  $B_y$  and  $B_z$  components in GSM coordinates,  $Dst$  index, and two averaged interplanetary parameters  $G_1$  and  $G_2$  given by the following equations,

$$G_1 = \langle h V_x \sin^3(\theta_c/2) \rangle, \quad (9a)$$

$$G_2 = a \langle V_z B_s \rangle, \quad (9b)$$

$$h = \frac{(B_{\perp}/B_c)^2}{(1 + B_{\perp}/B_c)}, \quad (9c)$$

$$B_{\perp} = \sqrt{B_y^2 + B_z^2}, \quad (9d)$$

where  $V_x$  is the  $x$  component of the solar wind velocity,  $\theta_c$  is the IMF clock angle,  $B_c = 40$  nT,  $a = 0.005$ , and  $B_s = |B_z|$  for  $B_s \leq 0$  or 0 otherwise. The averaging is done over the previous hour. Parameter  $G_1$  controls the strength of the near-Earth lobe field, while  $G_2$  controls the distance to the tail current, as well as the amplitude and scale size of the region 1 and region 2 field-aligned currents. Formally,  $G_1$

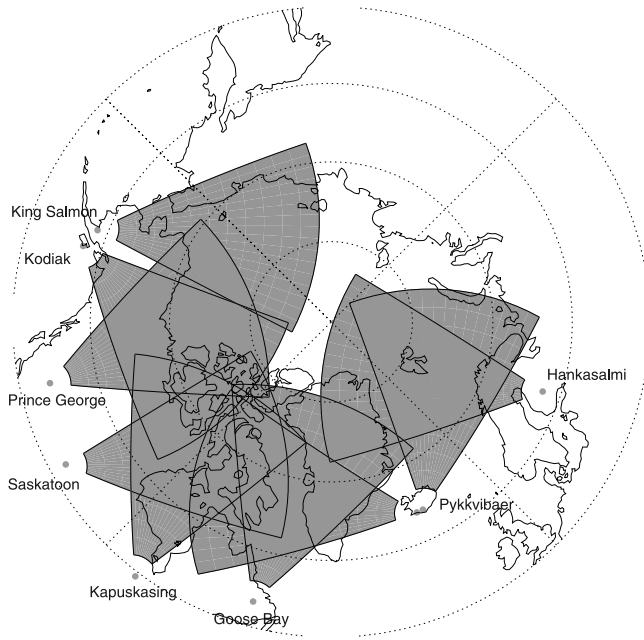


**Figure 1.** Combined field of view for the nine Northern Hemisphere SuperDARN radars. Concentric circles represent  $10^\circ$  increments of geographic latitude outward from the pole.

and  $G_2$  have the dimensionality of velocity and electric field, respectively. However, their normalizations were chosen somewhat arbitrarily to impose a dynamic range that has no stand-alone physical meaning. Furthermore,  $G_1$  includes a nonlinear dependence on  $B_\perp$  and  $\theta_c$ , while  $G_2$  could, in principle, be defined dimensionless. For these reasons, it is in some sense inappropriate to assign specific units to either parameter, and we will instead treat them both as ad hoc dimensionless indices. It should also be noted that correction of the  $Dst$  index for the effect of the solar wind dynamic pressure is done internal to the T01 model.

### 3.2. Electron Drift Instrument

[15] The ESA Cluster mission became operational in February 2001 and comprises four identical spacecraft in high-inclination elliptical orbits with apogee  $\sim 20 R_E$  and perigee  $\sim 4 R_E$ . The four spacecraft fly in formation with an interspacecraft separation that typically varies from 100 to 18,000 km [Escoubet et al., 2001]. During March 2001, the separation distances were approximately 800 km. The Cluster EDI measures the drift velocity of magnetospheric plasma by tracking a 0.5- or 1.0-keV electron beam injected perpendicular to the local magnetic field [Paschmann et al., 2001]. The EDI technique makes use of the fact that a drifting electron beam returns to the spacecraft only when fired in unique directions. Once these directions have been identified, the drift velocity can be deduced from the electron guiding center drift velocity by either “triangulation” [Quinn et al., 2001] or “time-of-flight” analysis [Paschmann et al., 2001]. EDI consists of two gun-detector units (GDUs) and a controller unit. The GDUs are mounted on opposite sides of the spacecraft with oppositely directed fields of view. The electron guns can fire in any direction within a hemisphere, thereby allowing measurement of any

arbitrary electric field configuration. As many as several hundred return beams can be received per spacecraft spin, depending on conditions.

[16] The EDI technique provides a full measurement of  $\mathbf{E}_\perp$ , the electric field perpendicular to the magnetic field. This represents an advantage over traditional double-probe instruments that measure the component of  $\mathbf{E}_\perp$  in the plane defined by the wire booms of the probe. Furthermore, double-probe measurements may, in some cases, become contaminated by electric fields induced by spacecraft wakes, sheaths, and photoelectrons. EDI is less susceptible to these contaminations because it senses the electric field at a location removed from the spacecraft by a distance of one electron gyroradius (typically 3–5 km). However, there are a number of situations in which EDI can be expected to suffer a temporary loss of data. These include (1) loss of beam tracking due to rapid changes in the electric field or magnetic field direction and (2) signal-to-noise problems as a result of insufficient return beam strength and/or excessive fluxes of ambient electrons. All EDI data presented in this paper are one-spin (4-s) averages that have been corrected for the motion of the spacecraft. Quality flags have been assigned to the data (GOOD, CAUTION, or BAD) based on the distribution of all return beams measured within the one-spin integration time. Only GOOD and CAUTION data have been retained for use in this paper.

### 3.3. Super Dual Auroral Radar Network (SuperDARN)

[17] SuperDARN is an international collaborative network of high-latitude HF radars that measure coherent backscatter from decameter-scale ionospheric irregularities that are aligned parallel to the magnetic field direction. The Doppler shift of the backscatter is proportional to the line-of-sight component of the  $\mathbf{E} \times \mathbf{B}$  plasma drift in the scattering region [Villain et al., 1985; Ruohoniemi et al., 1987]. At the present time there are nine SuperDARN radars in the Northern Hemisphere and six in the Southern Hemisphere. Figure 1 shows the combined fields of view of the Northern Hemisphere radars. A detailed description of SuperDARN as it existed at the start of the International Solar Terrestrial Physics (ISTP) mission is given in the work of Greenwald et al. [1995]. In brief, SuperDARN radars utilize an array of electronically phased antennas that can be steered in 16 beam directions across an azimuth sector of  $50^\circ$ . A variety of multipulse sounding sequences are used to unambiguously determine the range and Doppler velocity of the irregularities, while a secondary antenna array provides vertical angle-of-arrival information that can be used to determine their altitude. All SuperDARN radars operate continuously (except for very infrequent data outages) and typically operate at a temporal resolution of 1–2 min. All results presented in this paper are at 2-min resolution.

[18] Ruohoniemi and Baker [1998] developed an analysis procedure that combines all available SuperDARN Doppler data within a hemisphere and determines a solution for the ionospheric electrostatic potential as a weighted least squares fit to a spherical harmonic expansion of associated Legendre functions. The ability of the radars to measure velocities at a given location is dependent on the presence of magnetic-field-aligned irregularities to backscatter the radar signal. Other reasons why the radars might not measure

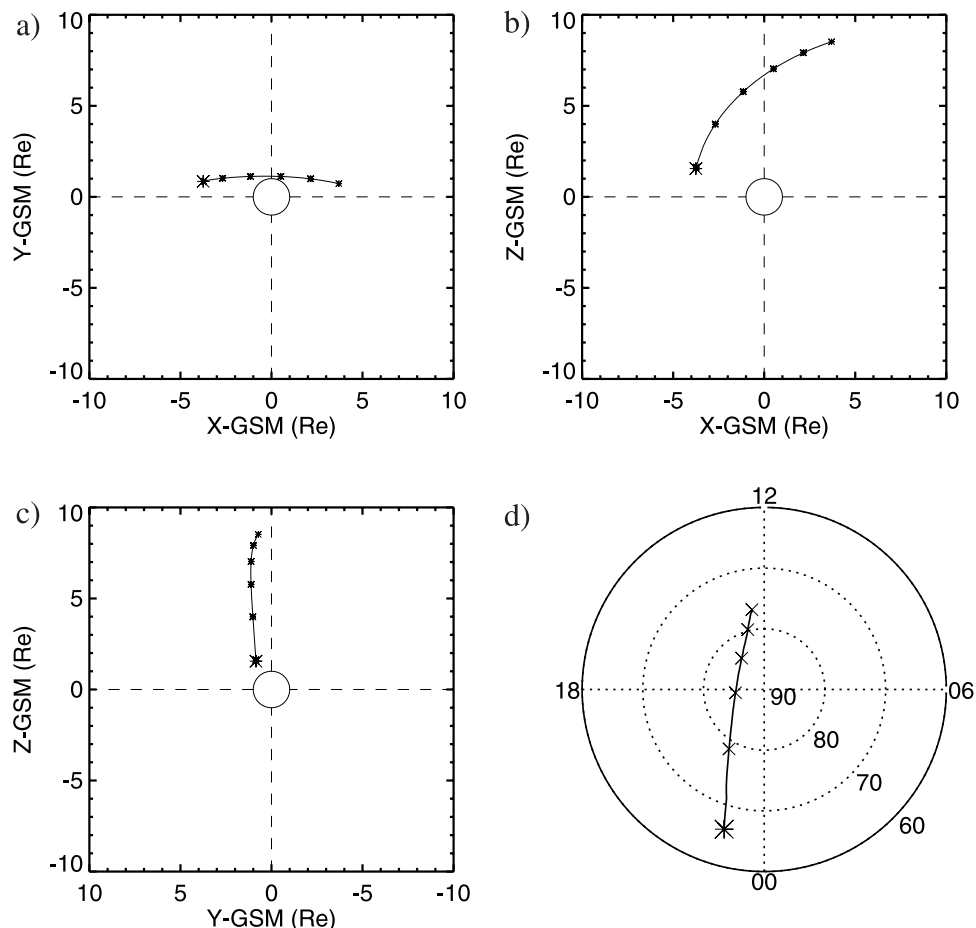


**Figure 2.** (a)–(c) Orbit of the Cluster-3 spacecraft from 0700 to 1200 UT on 12 March 2001. The starting location is represented as an asterisk, and the locations at hourly intervals are shown with small stars. (d) The ground track of T01 magnetic foot points in the Northern Hemisphere ionosphere at an altitude of 400 km. This plot is in AACGM MLAT-MLT format; magnetic noon is toward the top, and the lowest latitude shown is  $60^\circ$ .

ionospheric velocities at a particular location include (1) auroral absorption of the signal along the propagation path, (2) propagation conditions that prevent the radar signal from reaching a given location, and (3) clutter at some ranges from backscatter off the ground. In regions where backscatter is not available, the drift velocity can be estimated from the statistical convection models of *Ruohoniemi and Greenwald* [1996].

#### 4. Event Analysis: 0700–1200 UT on 12 March 2001

[19] We now use the formalism described in section 2.2 to compare SuperDARN and Cluster EDI drift measurements during 0700–1200 UT on 12 March 2001. For simplicity, we confine our attention to Cluster EDI data obtained from the Cluster-3 spacecraft. The particular event period was chosen because it provided simultaneous conjugate SuperDARN and EDI measurements for an extended period of time. We focus our attention on the following four subevent intervals when there were significant EDI-SuperDARN inconsistencies: A, 0730–0745; B, 0930–1000; C, 1005–1020; and D, 1100–1145 UT. An

effort will be made to reconcile the inconsistencies in terms of possible sources.

[20] The trajectory of the Cluster-3 spacecraft during the event interval is shown in Figure 2. Figures 2a–2c show planar projections of the Cluster-3 orbit onto the GSM axes. Figure 2d shows the track of ionospheric foot points obtained by mapping from the Cluster-3 location to the northern ionosphere using the T01 model. The foot points are plotted in magnetic latitude (MLAT) ( $\Lambda$ ) versus magnetic local time (MLT) format using the altitude adjusted corrected geomagnetic coordinates (AACGM) system of *Baker and Wing* [1989]. The minimum latitude shown is  $60^\circ$ , and magnetic noon is directed toward the top. During the event interval, the Cluster-3 spacecraft was crossing the northern polar cap at high altitude in an orbit that was approximately aligned along the midnight-noon meridian.

#### 4.1. T01 Model Input Parameters

[21] Interplanetary inputs to the T01 model were obtained from the Advanced Composition Explorer (ACE) spacecraft located in the solar wind  $\sim 227 R_E$  upstream of the Earth. IMF measurements were obtained from the ACE magne-

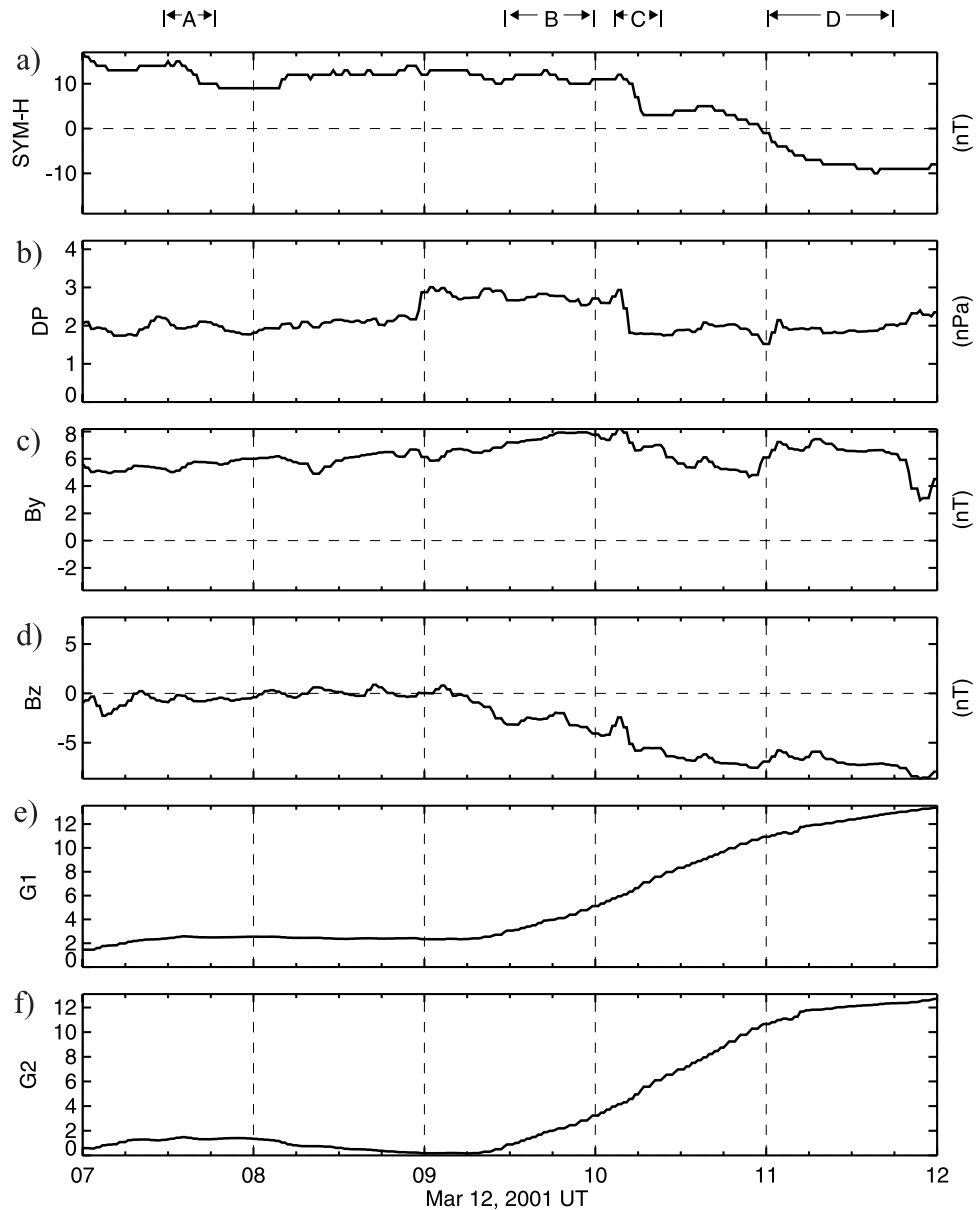


**Figure 3.** Time series of input parameters used to drive the T01 model during 0700–1200 UT on 12 March 2001. The spans of the subevent periods A–D are provided at the top. The parameters from top to bottom are (a) SYM-H index, (b) solar wind dynamic pressure, (c) IMF  $B_y$ , (d) IMF  $B_z$ , (e)  $G_1$ , and (f)  $G_2$  parameters.

tometer (MAG) instrument [Smith *et al.*, 1998], while solar wind plasma data were obtained from the solar wind electron, proton and alpha monitor (SWEPAM) instrument [McComas *et al.*, 1998]. Figure 3 displays time series plots for the six T01 input parameters during the event interval. The time spans of the subevent intervals A–D are identified at the top of the plot for later reference. All input parameters have been interpolated to a common resolution of 1 min. From top to bottom the parameters are SYM-H index, solar wind dynamic pressure, IMF  $B_y$  and  $B_z$  (GSM coordinates), and  $G_1$  and  $G_2$  parameters. The SYM-H index is a 1-min average of the  $H$  component magnetic disturbance measured by midlatitude magnetometers and can be considered a high-resolution version of the hourly  $Dst$  index [Iyemori and Rao, 1996]. The interplanetary parameters have been

shifted by a 67-min transit time to account for propagation of the solar wind from the ACE location at  $(227, -38, \text{and } -9) R_E$  in the solar wind to the Cluster-3 location within the magnetosphere. The transit time was calculated by matching the foot of a reduction in the  $B_x$  component of the geomagnetic field measured by the Cluster-3 fluxgate magnetometer (FGM) instrument [Balogh *et al.*, 1997] at 1010–1014 UT with the foot of a reduction in solar wind pressure measured at 0907 UT by ACE (see Figure 4). This transit time is slightly larger than the 65-min transit time obtained by using a magnetopause standoff distance of  $10 R_E$  and assuming ballistic propagation of the solar wind at the measured  $x$  component velocity of  $V_x \sim 360$  km/s. During the event interval, the IMF  $B_y$  component was steady and positive, while the  $B_z$  component made a transition from steady

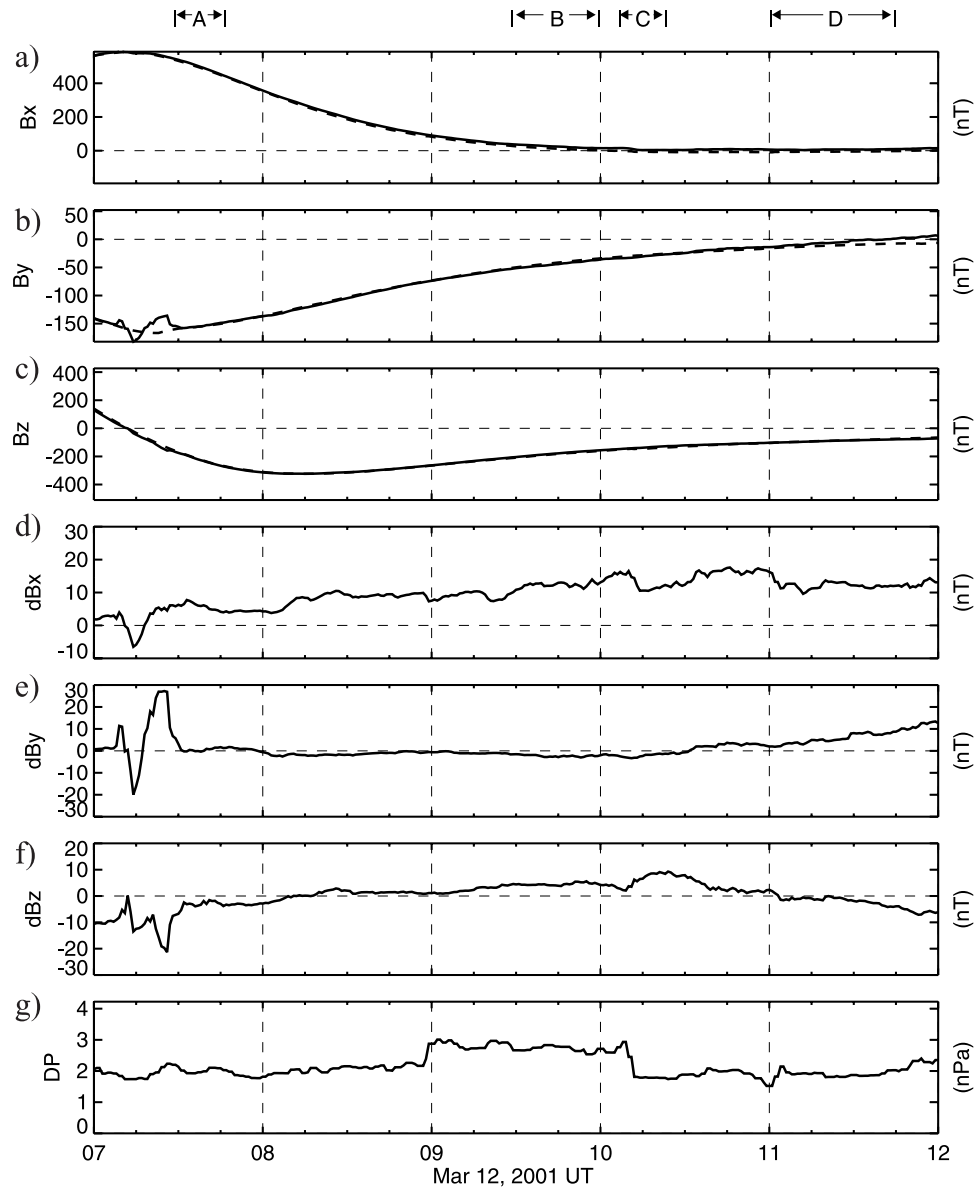


**Figure 4.** T01 model values compared with FGM measurements at Cluster-3. GSM (a)  $B_x$ , (b)  $B_y$ , and (c)  $B_z$  components of the geomagnetic field measured by FGM (solid) and according to the T01 model (dashed). (d)–(f) The differences between the FGM and T01 values. (g) The time-shifted solar wind dynamic pressure. The time spans of the subevent intervals A–D are provided at the top of the figure.

near-zero values to become increasingly negative after 0900 UT.

#### 4.2. Cluster FGM Measurements

[22] The accuracy of the technique developed in section 2.2 is dependent on the ability of the magnetic field model to correctly specify the magnetic conjugacy. An obvious quality check on the accuracy of the model during the event is to examine how closely it reproduces the magnetic field measured at the Cluster-3 location by the FGM instrument. This is done in Figure 4. Figures 4a–4c show the GSM  $B_x$ ,  $B_y$ , and  $B_z$  components of the magnetic field measured by FGM (solid) and the corresponding T01 model estimates (dashed); Figures 4d–4f show the differences between the measured and modeled values

(GSM  $dB_x$ ,  $dB_y$ , and  $dB_z$ ); and Figure 4g shows the time-shifted solar wind dynamic pressure. The time spans of the subevent intervals A–D are again provided across the top of the figure. There is a good agreement between the T01 model and FGM measurements throughout much of the event interval, but there are also notable discrepancies. In particular, the bipolar perturbations in the  $B_y$  component measured by FGM between 0710 and 0730 UT are consistent with the spacecraft passing through the region 1 and region 2 field-aligned current sheets under moderate levels of geomagnetic activity [e.g., *Donovan, 1993*]. As noted in section 4.1, there was a sudden reduction in solar wind dynamic pressure measured by ACE at 0907 UT. Figure 4 shows that there was a drop in GSM  $B_x$

**Table 1.** Minimum and Maximum Values of the T01 Input Parameters

	$Dst$ , nT	DP, nPa	$B_{10}$ , nT	$B_{20}$ , nT	$G_1$	$G_2$
Minimum	-100	0.5	-10	-10	0	0
Maximum	20	10	10	10	30	30

measured by the Cluster-3 FGM instrument at approximately 1014 UT that can be attributed to the pressure decrease measured 67 min earlier at ACE.

[23] At approximately 0900 UT the T01 foot point of Cluster-3 crossed the dawn-dusk meridian, and the  $B_x$  component measured by FGM became very small, but remained positive, as Cluster-3 continued moving toward the dayside magnetopause. The modeled T01  $B_x$  component, though also small, made a transition from positive to negative values at approximately 1000 UT. One plausible interpretation of this discrepancy is that the T01 model incorrectly estimates a crossing of the high-altitude boundary between the open field lines of the tail lobe and the closed field lines of the dayside magnetosphere. The consistent sunward direction of the magnetic field measured by FGM suggests that Cluster-3 was instead attached to the open tail lobe throughout the event interval. This discrepancy can perhaps be explained by the limitations of the T01 model parameterization. As explained in section 3.1, the location of the T01 magnetopause is dependent only on the instantaneous value of the solar wind dynamic pressure and dipole tilt angle. Motion of the dayside magnetopause associated with magnetic reconnection during extended periods of southward IMF is not included in the model. Figure 3 shows that the IMF had been southward for over 45 min at 1000 UT and continued to stay southward for the remainder of the event interval. It is thus likely that the dayside magnetic flux was significantly eroded by magnetic reconnection during this time. Under these circumstances, one might expect the T01 model to overestimate the amount of closed magnetic flux in the dayside magnetosphere. This is consistent with the fact that the T01 model incorrectly identified a transition from tailward to sunward directed magnetic field lines along the Cluster-3 trajectory.

[24] The accuracy of the T01 estimate for the Cluster-3 magnetic field can be improved by tweaking the input parameters to produce better agreement with FGM measurements. One might hope that the tweaked input parameters will produce a more accurate mapping to the ionosphere. However, this is not necessarily the case because there may be a large number of T01 input parameter combinations that reproduce the FGM measurements more accurately but nevertheless produce very different mappings to the ionosphere. Choosing which particular set of tweaked input parameters to use would then be somewhat arbitrary. Nevertheless, this type of tweaking analysis provides a valuable check on the sensitivity of the T01 model to its input parameters and can provide qualitative error estimates on the location of the foot points. Table 1 shows the upper and lower limits (or dynamic ranges) of the six input parameters for which the T01 model is valid. The first step in the tweaking analysis is to normalize the T01 input parameters to their respective dynamic ranges so that each input is expressed on a scale between 0 and 1. New sets of

input parameters are considered by defining a tweaking factor,  $T$ , to be the root-mean square deviation of the new inputs from the nominal T01 inputs expressed in the normalized six-dimensional parameter space. All possible sets of input parameters corresponding to a particular value of  $T$  were considered. Any sets of tweaked inputs that contained one or more input values that fell outside the dynamic ranges specified in Table 1 were immediately discarded as being beyond the working limitations of the T01 model. All other input combinations were tested to see if they produced better agreement with the FGM measurements. The input parameters were then ranked according to the mean square deviation of the T01 outputs from the FGM measurements. Field line mappings to the ionosphere were produced for the leading 1000 sets of tweaked input parameters, and the spatial offset from the location of the nominal T01 foot point to the tweaked foot point was calculated. This process was repeated for each 2-min interval during the entire event using different values for the tweaking factor,  $T$ .

[25] Figure 5 shows the results of this tweaking analysis. The difference between FGM measurements and T01 model estimates is shown for the leading 1000 sets of tweaked input parameters. Figures 5a–5d show the  $dB_x$ ,  $dB_y$ ,  $dB_z$ , and  $dB$  offsets in the magnetic field (GSM coordinates) at Cluster-3, while Figure 5e shows the spatial offset from the nominal T01 foot point location in the ionosphere. Each point has been colored according to the minimum tweaking factor,  $T$ , as measured by the color scale at the right. Also plotted in red are the results obtained by using the nominal T01 input parameters, while those plotted in black are the optimal results. The analysis was not carried out for the interval immediately prior to 0730 UT when the Cluster-3 FGM instrument measured the effects of the region 1 and region 2 field-aligned currents. For most of the rest of the event period, it can be seen that tweaking the T01 inputs produces improved T01 output values that agree with the FGM measurements to within 1–2 nT. Furthermore, in many cases, this improved agreement is obtained with relatively small values for the tweaking factor and spatial offset. However, it is interesting to note that during the last hour of the event interval no amount of tweaking can completely correct the offset in the  $B_y$  component. Figure 5e shows that the magnitude of the spatial offset in the ionosphere increases as the Cluster-3 spacecraft moves toward the dayside magnetopause, and the T01 model output becomes relatively more sensitive to variation of its input parameters. Assuming that the geomagnetic field is accurately represented by the input parameter space spanned by the T01 model, it is therefore reasonable to expect a maximum error of 400 km for the T01 foot point locations during the entire event interval.

### 4.3. SuperDARN Ionospheric Convection Patterns

[26] Figure 6 shows ionospheric convection patterns obtained from the *Ruohoniemi and Baker* [1998] electrostatic potential analysis of SuperDARN data at four different times during the event period: 0734, 0946, 1010, and 1130 UT. These times were chosen to be representative of the ionospheric convection during each of the subevent intervals A–D, respectively. Line-of-sight velocity mea-

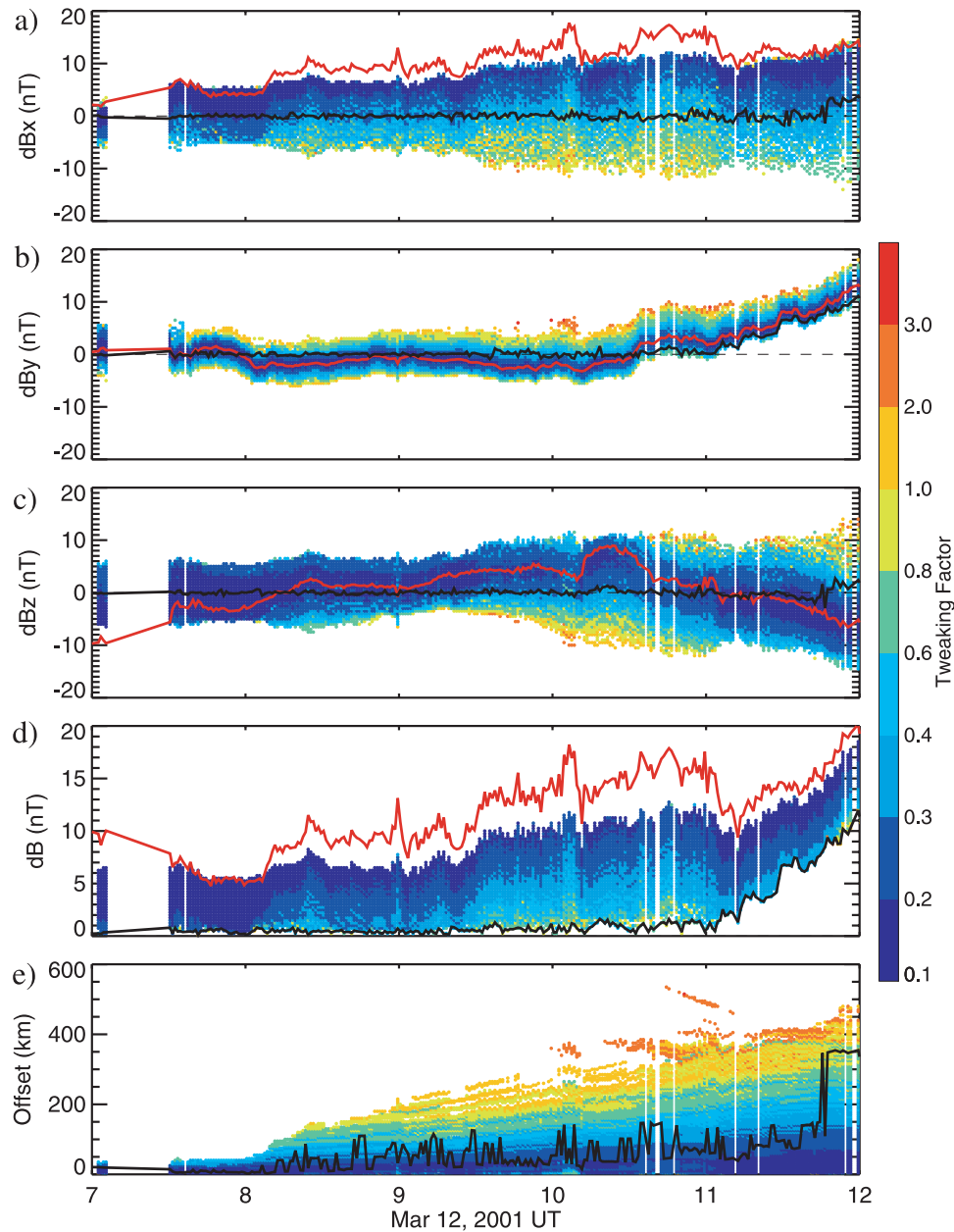


**Figure 5.** Differences between FGM measurements and T01 model estimates using 1000 sets of tweaked T01 input parameters (see section 4.2): (a)  $dB_x$ , (b)  $dB_y$ , (c)  $dB_z$ , and (d)  $dB$  (GSM) magnetic offsets at Cluster-3 and (e) corresponding spatial offsets in the ionosphere. The color scale represents the amount of tweaking in a normalized parameter space. Red curves show the nominal T01 values; black curves show the optimal results. The presence of field-aligned currents produces a gap in the analysis immediately prior to 0730 UT.

measurements from seven Northern Hemisphere SuperDARN radars contributed toward the calculation of each pattern over a 2-min integration time. The results are presented in the same AACGM Sun-fixed  $\Lambda$ -MLT format that was used in Figure 2d. The minimum latitude is  $60^\circ$ , and magnetic noon is directed toward the top. Negative (positive) potential contours are displayed as solid (dashed) lines, and the contour spacing is 6 kV. Self-consistent velocity vectors are overplotted in locations for which line-of-sight velocity measurements were obtained by one or more SuperDARN radars and are colored according to the velo-

city scale at the right. For each convection image, the instantaneous location of the T01 ionospheric foot point for the magnetic field line threading the Cluster-3 spacecraft is identified as a small triangle. In addition, the locations of Fort Smith, Canada ( $60.03^\circ\text{N}$ ,  $248.07^\circ\text{W}$ ), and Ny Alesund (NAL), Norway ( $78.92^\circ\text{N}$ ,  $11.95^\circ\text{E}$ ) are identified by asterisks on the images at 0734 and 1010 UT, respectively. It can be seen that Cluster-3 was closely conjugate to these locations at these times. In section 4.4, ground-based measurements obtained from these locations will provide contextual information for the comparison of

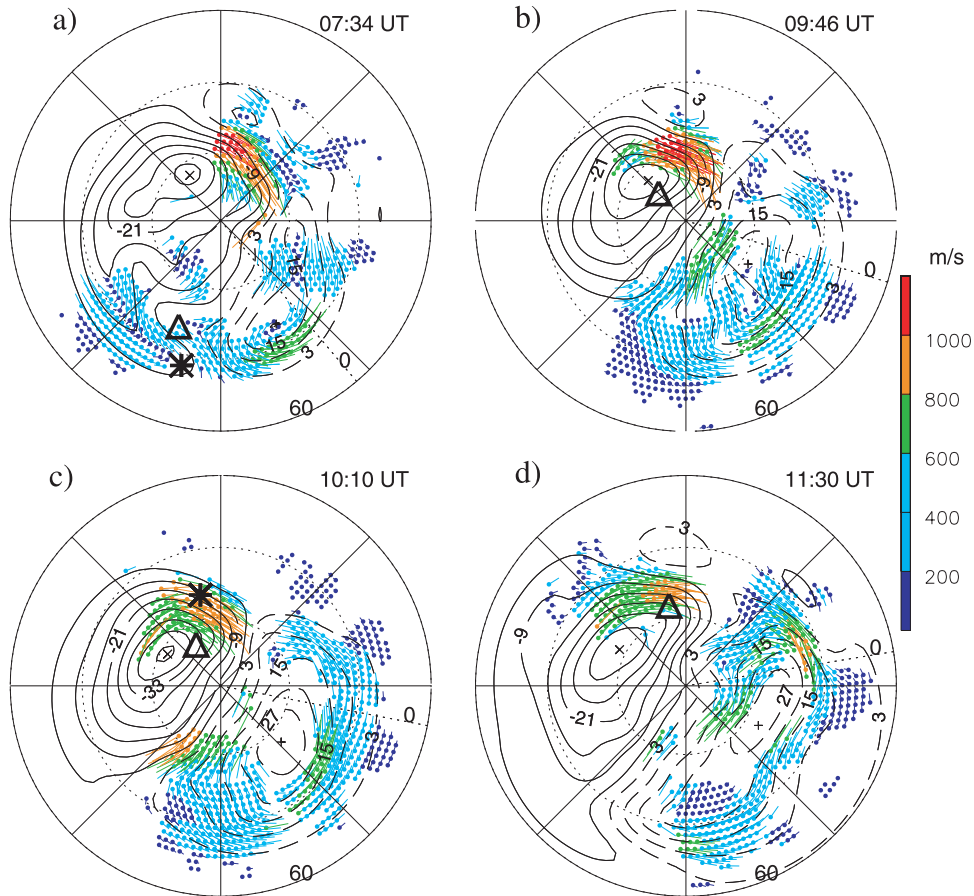


**Figure 6.** SuperDARN ionospheric convection patterns at (a) 0734, (b) 0946, (c) 1010, and (d) 1130 UT in AACGM magnetic clock dial format (noon is directed upward). The patterns characterize conditions during the subevent periods A–D, respectively. Contours show the electrostatic potential at a spacing of 6 kV. Self-consistent velocity vectors are provided at locations where line-of-sight velocity measurements were obtained (color scale at right). The ionospheric foot point of the Cluster-3 spacecraft is identified as a small triangle. The locations of Fort Smith, Canada (60.03°N, 248.07°W), and NAL, Norway (78.92°N, 11.95°E) are identified by asterisks on the images at 0734 and 1010 UT, respectively.

EDI and SuperDARN observations during intervals A and C.

#### 4.4. Electrostatic Conjugate Comparison of EDI and SuperDARN Measurements

[27] In this section, measurements of  $\mathbf{E} \times \mathbf{B}$  drift obtained from SuperDARN and Cluster EDI will be compared with each other during the 12 March 2001 event. Following the formalism developed in section 2.2, the magnetic field lines,  $L_i$ , are chosen such that  $L_0$  initiates at the instantaneous location of Cluster-3, while the starting points of  $L_1$  and  $L_2$  are each displaced a distance  $\Delta l$  from Cluster-3 along the GSM  $x$  and  $y$  directions, respectively. A value of  $\Delta l = 0.1 R_E$  was chosen so that the separation of the  $L_i$  foot points in the ionosphere was less than the spatial resolution of the grid used in the *Ruohoniemi and Baker* [1998] analysis of SuperDARN data ( $\sim 110$  km). This choice was in keeping with the assumption that the electric and magnetic fields are constant across the bundle of magnetic field lines. The values of electrostatic potential,  $\Phi_i^e$ , are assigned to the magnetic field lines from the *Ruohoniemi and Baker*

[1998] analysis, based on the locations of the T01 ionospheric foot points at an altitude of 400 km. It should be stressed that  $\Phi_i^e$  have been corrected for corotation and are expressed in the same Sun-fixed GSM coordinates that are used for the Cluster-3 measurements. Finally, the value for the magnetic field,  $\mathbf{B}_0$ , at the Cluster-3 location is provided by the Cluster FGM measurements. With these quantities specified, equations (8a)–(8c) are used to obtain a SuperDARN estimate for the drift velocity at Cluster-3 that can be compared directly with the EDI measurements.

[28] The results of the SuperDARN-EDI plasma drift comparison for 0700–1200 UT on 12 March 2001 are shown in Figure 7. Figures 7a–7c show the  $V_x$ ,  $V_y$ , and  $V_z$  GSM components of  $\mathbf{E} \times \mathbf{B}$  drift; Figure 7d is the drift velocity magnitude ( $V$ ); Figure 7e is the distance from the T01 ionospheric foot point to the nearest SuperDARN line-of-sight velocity measurement ( $dR$ ); and Figure 7f is the time-shifted solar wind dynamic pressure. In Figures 7a–7d the Cluster EDI measurements sampled at the spin period of the spacecraft (4-s) are plotted in blue, while the SuperDARN ionospheric measurements

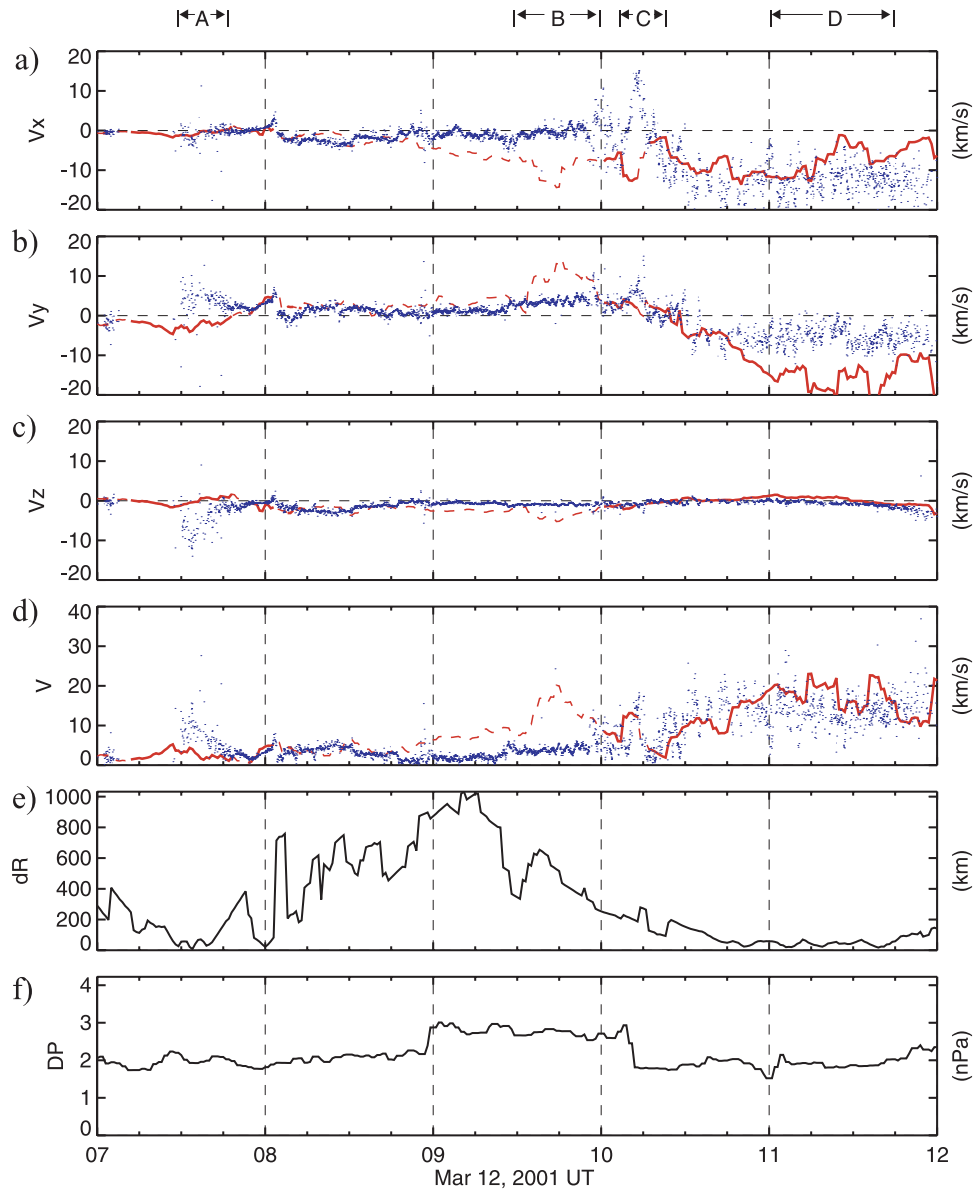


**Figure 7.** Direct comparison of EDI (blue) and SuperDARN (red) measurements of  $\mathbf{E} \times \mathbf{B}$  plasma drift. SuperDARN measurements have been mapped upward along T01 magnetic field lines to the Cluster-3 location: GSM (a)  $V_x$ , (b)  $V_y$ , and (c)  $V_z$  drift components; (d) drift magnitude,  $V$ ; (e)  $dR$ , the distance from the T01 ionospheric foot point to the nearest SuperDARN line-of-sight velocity measurement; and (f) solar wind dynamic pressure.

mapped to the location of Cluster-3 using the T01 model are shown at a resolution of 2 min in red. Solid red lines are used for times when SuperDARN line-of-sight velocity measurements were available within 250 km of the Cluster-3 foot point (i.e.,  $dR < 250$  km); dashed red lines are used otherwise. This cutoff value for  $dR$  was chosen arbitrarily to represent periods of time when the ionospheric electric field is well defined by SuperDARN measurements at the foot point location. This distinction is important because the ionospheric electrostatic potential obtained from the *Ruohoniemi and Baker [1998]* analysis is a combination of SuperDARN line-of-sight velocity measurements where available and statistical models otherwise. The degree of correspondence between SuperDARN and EDI at any given time is thus dependent on

the extent to which the SuperDARN radars are able to measure convection velocities in the vicinity of the Cluster-3 foot point.

[29] Figure 7 shows good general agreement in the trend of EDI and SuperDARN drift velocities throughout much of the event interval. For example, both data sets show an increase in the strength of antisunward convection during the latter part of the event when the IMF became southward. However, there are also intervals in which there are noteworthy differences. The most prominent of these fall within the periods labeled by the letter classifications A–D. The remainder of this paper is focused on identifying possible sources for these inconsistencies. One of the more obvious sources might be the accuracy with which the T01 model can identify the location of the Cluster-3 foot point in the

ionosphere. Possible errors in the T01 mapping could take two forms. First, the relative geometry of the “true” ionospheric foot points in the bundle of magnetic field lines  $L_i$  might be twisted with respect to the T01 model foot points. The other possibility is that the true foot points might be collectively translated from the T01 foot points by some small distance. This second, much simpler, possibility is considered in some detail in the next section.

#### 4.5. Optimized T01 Ionospheric Foot Points

[30] In section 4.2, it was demonstrated that the difference between the FGM magnetic field measurements at Cluster-3 and the T01 estimates using the nominal range of input parameters could be responsible for producing errors in ionospheric foot point location as large as 400 km. We now investigate the effect that small offsets of this magnitude might have on the consistency between the EDI and SuperDARN drift measurements. We assume that the relative geometry of the  $L_i$  foot points is conserved and seek the magnitude and direction of a small spatial offset in the ionosphere, that when applied collectively to the field line bundle produces improved correspondence between the EDI and SuperDARN observations. A small circular area centered on the nominal T01  $L_0$  foot point location is searched for the ionospheric location at which the SuperDARN  $\mathbf{E} \times \mathbf{B}$  drift velocity has the smallest root-mean-square deviation from the EDI-measured velocity. If an improved foot point location is identified within the search area, then the drift velocity at the nominal T01 foot point is replaced with the velocity from the new (or “optimized”) foot point. Figure 8 shows the improved results that can be obtained by performing this simple procedure. Figures 8a–8c show the  $V_x$ ,  $V_y$ , and  $V_z$  GSM components of plasma drift at Cluster-3. Black curves represent EDI measurements averaged to the 2-min resolution of the SuperDARN measurements. Multiple colors are used to represent SuperDARN estimates obtained from optimized foot points within different-sized search areas. Blue, green, and red curves, respectively, represent search areas with radii of 100, 200, and 400 km, respectively. Figures 8d and 8e show the magnetic latitude and local time of the nominal  $L_0$  foot point (black) and optimized foot points (colored). The subevent intervals A–D are again shown along the top of the figure for reference.

[31] The results in Figure 8 demonstrate that searching for optimized foot point locations can sometimes produce significant improvement in the consistency between EDI (black) and SuperDARN (colored) observations. However, it should be cautioned that the technique provides only a qualitative improvement because there is no guarantee that the optimized T01 foot point is the true magnetic foot point appropriate to the particular magnetospheric conditions at any given time. Indeed, it is likely that in some instances the search for optimized foot points may produce EDI-SuperDARN correspondence that is artificially closer than it should be. Nevertheless, the technique does provide some valuable qualitative information about the performance of the T01 model. During some periods the black and colored curves converge as the search area widens, indicating that the inconsistencies between SuperDARN and EDI can probably be attributed, at least in some part, to errors in the T01 magnetic mapping. This convergence is particularly

evident during interval D when Cluster-3 was conjugate to the noon-sector “convection throat” region. By contrast, during intervals A and C the technique yields only modest improvements in consistency as the search area widens. This suggests that foot point displacement is not the primary explanation for the inconsistencies during these intervals.

## 5. Discussion

[32] We now discuss the EDI and SuperDARN measurements during each of the subevent intervals A–D in some detail and attempt to reconcile the inconsistencies in terms of limitations of the T01 model or the presence of parallel and/or inductive electric fields. Where appropriate, the consistency between Cluster-3 measurements and those obtained on the other Cluster spacecraft is discussed. In some cases, observations from ground-based measurements provide additional contextual information about the geomagnetic conditions on magnetic field lines in the vicinity of Cluster-3.

### 5.1. Interval A (0730–0745 UT)

[33] During interval A the Cluster-3 spacecraft was conjugate to the premidnight auroral zone at  $\sim 70^\circ$  magnetic latitude (see Figure 2). Figure 7 shows large inconsistencies in the strength and direction of the plasma flow measured by EDI and derived from SuperDARN. EDI observed large flows toward the central plasma sheet ( $-Z$ ) and dusk ( $+Y$ ), whereas the projected SuperDARN flows were of lesser magnitude and predominantly toward dawn ( $-Y$ ). This discrepancy occurred despite the fact that SuperDARN line-of-sight velocity measurements were available in the close vicinity of the Cluster-3 ionospheric foot point as specified by T01 during this period. Moreover, the foot point optimization technique did not yield significant improvement in the agreement between the EDI and SuperDARN data sets (see Figure 8). It is therefore tempting to consider a geophysical source for the inconsistency that might be associated with the field-aligned currents measured by FGM just prior to interval A at 0710–0730 UT (see Figure 4). *Donovan* [1993] has shown that moderate field-aligned currents (200 nT at 800 km) can shift the ionospheric foot point of magnetic field lines by up to 0.3 hours of magnetic local time. However, a collective translation of foot points of this magnitude is within the range evaluated in the optimized foot points procedure and is therefore insufficient to explain the inconsistency. The results therefore suggest that if the inconsistency is associated with a distorted field-line mapping due to the effects of the field-aligned current, then the bundle of field lines must have been twisted with respect to the T01 model.

[34] Other possibilities that may have affected the agreement during this period include partial decoupling of magnetospheric and ionospheric convection due to the presence of a spatially localized region of parallel electric field and/or the existence of an inductive electric field. As noted in the introduction, perpendicular gradients in parallel electric fields produce distortions in the mapping of convection between the magnetosphere and ionosphere [*Hesse et al.*, 1997]. Figure 9 shows measurements obtained from Canadian Auroral Network for the OPEN Program Unified Study (CANOPUS) instruments at Fort Smith, Canada

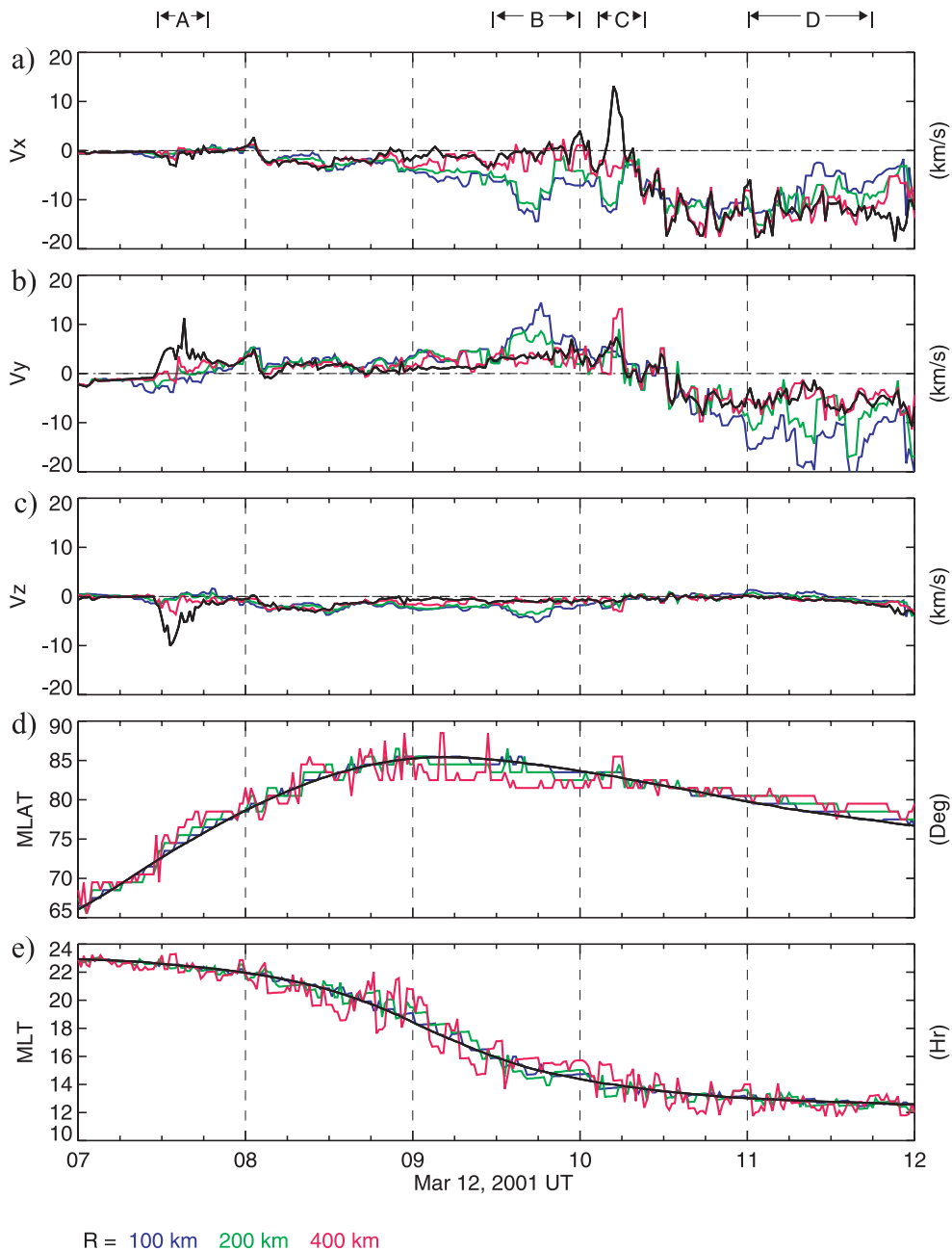


**Figure 8.** Results obtained from the optimized foot points technique (see text): GSM (a)  $V_x$ , (b)  $V_y$ , and (c)  $V_z$  drift components at Cluster-3 and (d) magnetic latitude and (e) local time in the conjugate ionosphere. Black curves show 2-min averages of EDI measurements. Blue, green, and red curves represent the most consistent SuperDARN results obtained within 100, 200, and 400 km of the nominal foot point, respectively.

(60.03°N, 248.07°W). The asterisk in Figure 6a identifies the MLAT-MLT location of Fort Smith, which was closely conjugate with Cluster-3 at 0734 UT. The parameters displayed in Figure 9 from top to bottom are meridian scanning photometer (MSP) brightness keogram at 557 nm,  $x$  component (geographic northward) magnetic disturbance, and riometer voltage (Note: decreased riometer voltage is indicative of increased ionospheric absorption, and hence >30 keV electron precipitation). Despite the fact that it was cloudy at Fort Smith, the CANOPUS measurements confirm that there was significant auroral activity during

interval A in the vicinity of the Cluster-3 foot point location. Vertical lines indicate two prominent auroral onsets at 0726 and 0741 UT that were measured by all three CANOPUS instruments. Figure 10 is a stackplot of the  $x$  component from six magnetometers in the east-west CANOPUS chain from Dawson (west) to Gillam (east). It provides a wider spatial context for the Fort Smith observations, and in particular, shows that the two auroral onsets identified by the vertical lines are merely two of a series of three to four regularly spaced (10–15 min) pseudo-onsets that precede the onset of a major substorm expansive phase, which

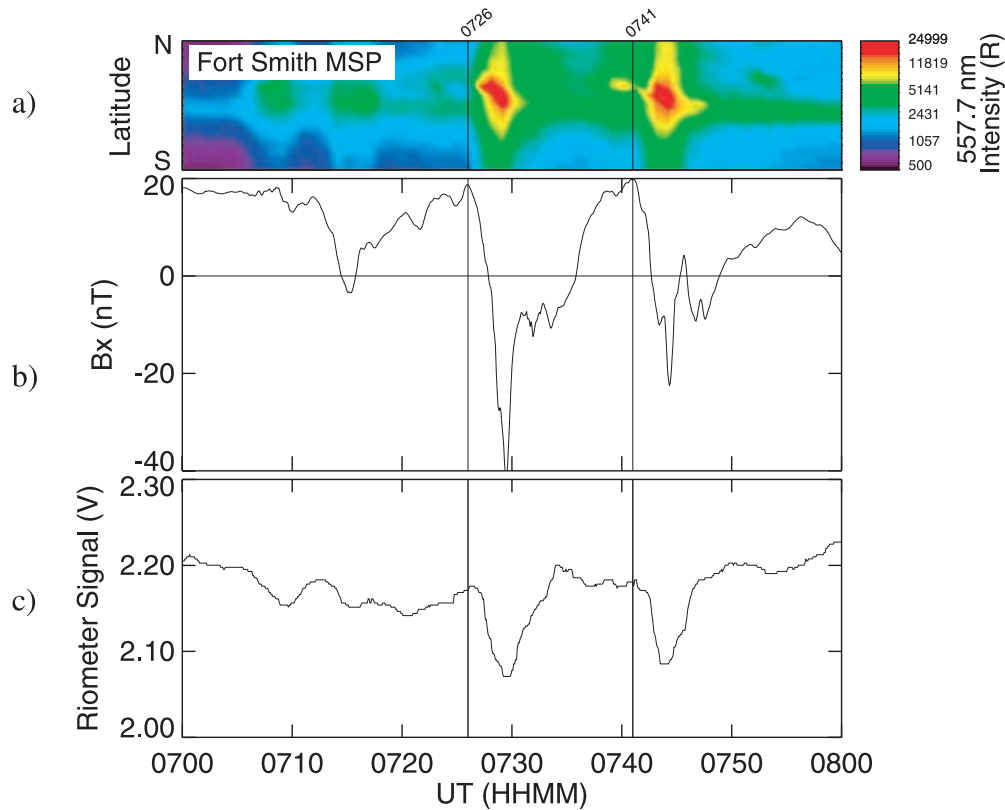


**Figure 9.** Time series of CANOPUS measurements obtained from Fort Smith, Canada ( $60.03^\circ\text{N}$ ,  $248.07^\circ\text{W}$ ). (a) A 557-nm brightness keogram from the meridian scanning photometer. The field of view of the photometer is  $160^\circ$  centered on the zenith. North is directed upward (N); south is downward (S). (b) The  $B_x$  (geographic northward) magnetic disturbance. (c) The riometer voltage. Vertical lines indicate auroral onsets at 0726 and 0741 UT.

initiates at approximately 0800 UT. These ground-based observations are therefore consistent with the presence of inductive and/or parallel electric fields in the vicinity of the Cluster-3 spacecraft during interval A. The weak convection measured by SuperDARN during interval A, when compared with EDI, is consistent with numerous observations showing weaker ionospheric electric fields and plasma flows at the location of active aurora relative to the wider vicinity [e.g., *Wescott et al.*, 1969; *Rino et al.*, 1974; *Weimer et al.*, 1994; *Yeoman et al.*, 2000; *Bristow et al.*, 2001]. One explanation for this phenomenon is that the magnetosphere may not be able to maintain current continuity during periods of enhanced auroral precipitation, necessitating the generation of parallel electric fields.

[35] We have also examined whether the measurements obtained by FGM and EDI on Cluster-3 are consistent with those obtained on the other Cluster spacecraft (Note: the Cluster-4 EDI did not collect data on this day). During interval A, Cluster-3 was separated from Cluster-1, Cluster-2, and Cluster-4 by distances of 532, 540, and 1010 km, respectively. Cluster-2, Cluster-3, and Cluster-4 followed similar trajectories, with Cluster-3 leading and Cluster-4 trailing. Cluster-1 was in a separate trajectory that led the other three spacecraft at a slightly higher altitude. FGM measurements from all four spacecraft show evidence of similar field-aligned current sheet crossings. The structure of the currents seen by Cluster-1 is somewhat different from

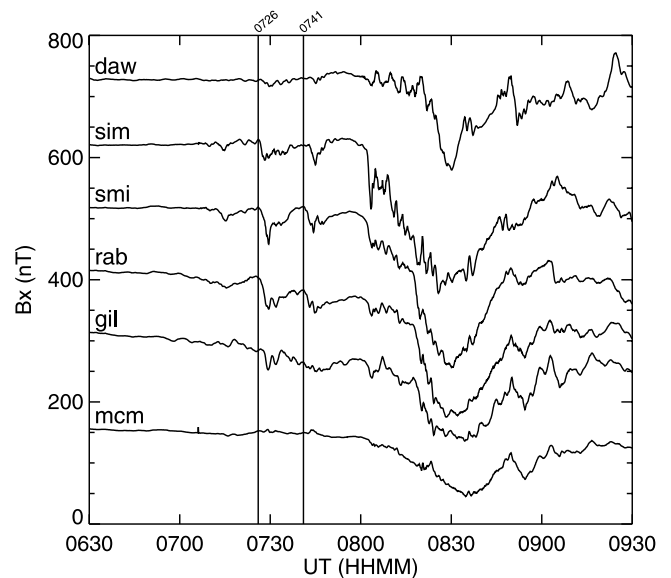


**Figure 10.** Stackplot of the  $x$  component (geographic northward) from magnetometers in the east-west CANOPUS chain. Vertical lines indicate auroral onsets at 0726 and 0741 UT.

those seen by the other spacecraft but this is consistent with it having a unique trajectory at a higher altitude. The FGM measurements on Cluster-2 and Cluster-4 are qualitatively similar to those from Cluster-3; however, there are slight differences that suggest temporal and/or spatial variations in the strength of the field-aligned currents. In particular, the currents measured by Cluster-2 and Cluster-4 are stronger than those measured by Cluster-3. This is consistent with the small-scale temporal and spatial variability of geomagnetic and auroral activity measured on the ground. Likewise, the EDI measurements on Cluster-1 and Cluster-2 are similar to those obtained on Cluster-3, in an average sense, if one neglects high-frequency variations and spikes. All three EDI instruments measured strong flows directed toward the plasma sheet and dusk.

[36] In summary, FGM measurements are consistent with a crossing of field-aligned current sheets just prior to interval A, and ground-based measurements show significant auroral precipitation and geomagnetic disturbance occurring on magnetic field lines connected to the Cluster-3 spacecraft. The region of inconsistency between SuperDARN and EDI is certainly spatially localized and perhaps temporally localized to some extent as well. Because there is a well-defined link between observations of auroral precipitation, field-aligned currents, and parallel electric fields [e.g., Knight, 1973; Olsson *et al.*, 1998] it is tempting to conclude that Cluster-3 passed through or above a localized region of parallel electric field at the poleward edge of the field-aligned current sheets. Inductive electric fields associated with substorm phenomena and twisting of the magnetic geometry by the presence of the field-aligned currents may also have contributed to the inconsistency.

### 5.2. Interval B (0930–1000 UT)

[37] During interval B the Cluster-3 ionospheric foot point was at the highest latitudes of the polar cap (see Figure 6b). The  $dR$  parameter was large, signifying poor coverage of SuperDARN convection measurements in the vicinity of the Cluster-3 ionospheric foot point. Under these circumstances, the SuperDARN estimates for the drift velocities at Cluster-3 are driven more by the statistical convection model of Ruohoniemi and Greenwald [1996], than actual measurements. The optimized foot points technique produces some improvement in the correspondence between EDI and SuperDARN, but the optimized foot point locations still lie within the area of poor spatial coverage. We are therefore hesitant to place too much significance on the improvement in this case. We instead conclude that the EDI-SuperDARN inconsistency probably has little or no geophysical significance during interval B and can be wholly attributed to inadequate spatial coverage of ionospheric convection in the vicinity of the Cluster-3 foot point.

### 5.3. Interval C (1005–1020 UT)

[38] During interval C the Cluster-3 spacecraft was at  $6.4 R_E$  altitude and its ionospheric foot point moved from the dayside polar cap toward the noon-sector auroral zone, approaching (but not yet entering) a region in which there was exceptional SuperDARN coverage of ionospheric convection (see Figure 6c). Just prior to 1000 UT, EDI started

to measure stronger flows in the sunward and antisunward directions (see Figure 7). At 1014 UT a particularly strong burst of sunward convection was measured that exceeded 17 km/s. We focus our attention on this largest burst of sunward convection. By comparison, the SuperDARN estimates for the convection at Cluster-3 during this time show increased convection in the antisunward, rather than sunward, direction. The strength of the burst and the short temporal scale over which it existed is very suggestive of a short-lived dynamic influence that might have operated in the magnetosphere during this time. If this were the case, then inductive electric fields associated with dynamic variations in the magnetic fields would not map to the ionosphere along magnetic field lines and could be responsible for EDI-SuperDARN inconsistencies.

[39] A possible source for the convection burst can be identified in the interplanetary measurements. Figure 3 shows a sudden decrease in solar wind dynamic pressure that impinged on the magnetosphere at approximately 1010–1014 UT. This was accompanied by transient increases in the IMF  $B_y$  and  $B_z$  components that may also have played a role in the generation of the flow burst measured at Cluster-3. The discussion here is focused on the decrease in pressure because it has the clearest step-like signature. We can be reasonably confident of the timing of the arrival of the pressure decrease at Cluster-3 because it produced a sudden 10–12 nT decrease in the strength of the GSM  $B_x$  component and a similar increase in the GSM  $B_z$  component measured by the FGM instrument at 1010–1014 UT (Figure 4 shows some of this variation relative to the T01 model magnetic field). The magnetic variations are consistent with a sunward springing of the magnetic field at Cluster-3 in response to the rapid drop in solar wind dynamic pressure. This sunward displacement would have an associated dawnward inductive electric field. If the magnitude of the inductive electric field were 1 mV/m, it would fully explain the burst of sunward velocity measuring 17 km/s, and the burst would not be observed in the ionosphere. The fact that a small burst was measured in the ionosphere suggests that there was an electrostatic component to the increased electric field observed at Cluster-3.

[40] During interval C the Cluster spacecraft were flying in a tetrahedron formation with Cluster-3 separated from Cluster-1, Cluster-2, and Cluster-4 by 265, 436, and 880 km, respectively. Cluster-3 was the most sunward of the spacecraft; it was trailed by Cluster-1 at a slightly higher altitude; while Cluster-2 and (last) Cluster-4 followed along a similar trajectory to Cluster-3. The magnetic response to the decrease in dynamic pressure was measured simultaneously by FGM on all four Cluster spacecraft (not shown). A similar but slightly weaker burst of sunward convection was measured by EDI on Cluster-1 and Cluster-2 at the same time as that observed at Cluster-3. There were some differences in fine structure between the bursts measured by EDI on all three spacecraft, particularly at the time when the main burst was decaying at 1015 UT and a smaller duskward burst was initiating (see Figure 7). This secondary duskward burst was also measured at Cluster-1 and Cluster-2 but at successive 30-s intervals later than it was at Cluster-3. We can therefore conclude that the secondary burst was spatially localized and/or might have

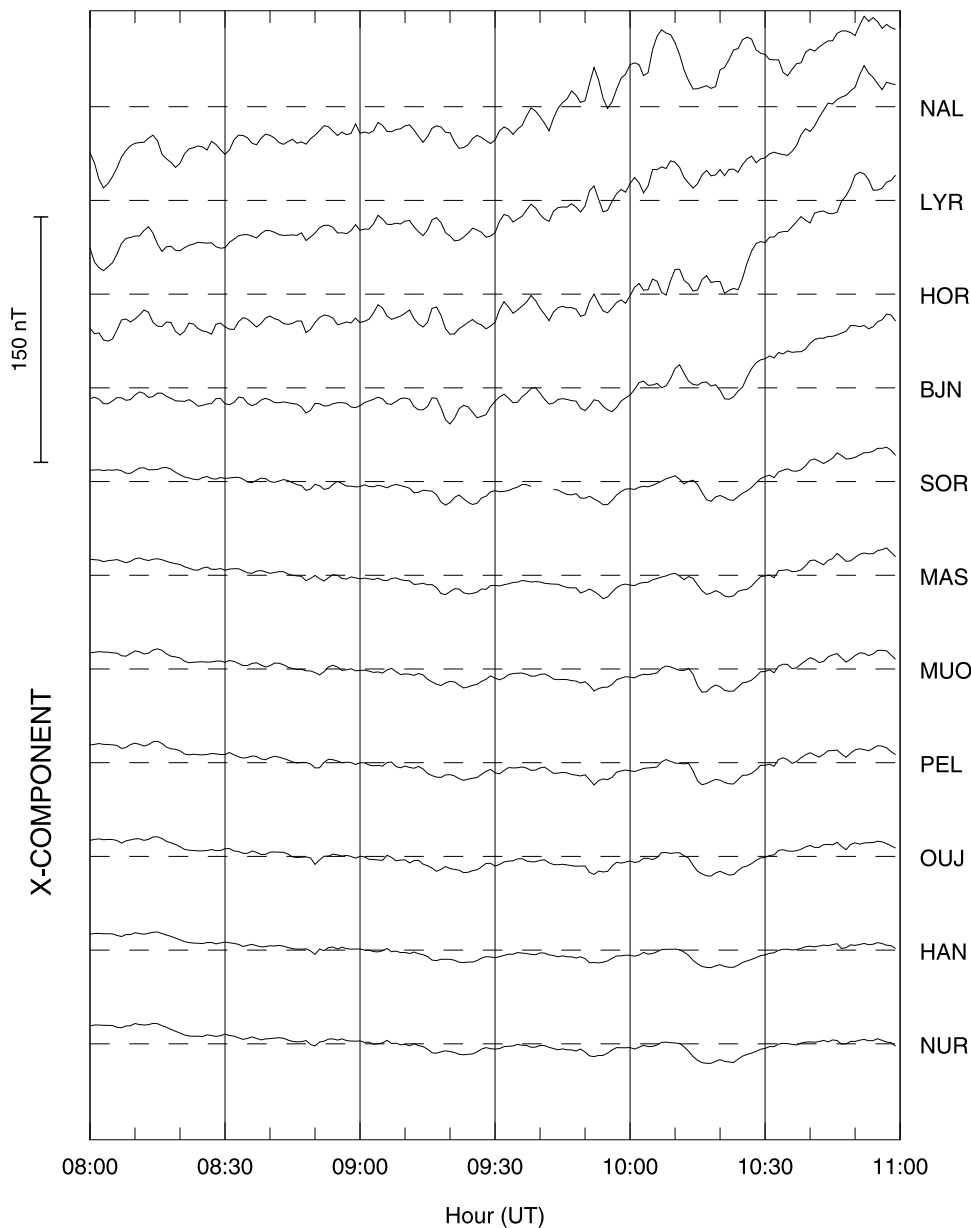


**Figure 11.** The  $X$  component (geographic northward) magnetic disturbance measured between 0800 and 1100 UT on 12 March 2001 by a north-south chain of IMAGE network magnetometers.

propagated between the spacecraft. However, over the 5-min timescale that the large sunward burst evolved, both FGM and EDI measurements were qualitatively similar and simultaneous on all spacecraft, suggesting that the primary sunward burst existed on a large spatial scale and may well have been associated with the magnetospheric response to the sudden reduction in solar wind dynamic pressure measured at ACE.

[41] Ground-based measurements from the IMAGE magnetometer network in Scandinavia show the decrease in dynamic pressure arrived at a time of preexisting high-latitude dayside geomagnetic activity. Figure 11 shows the  $x$  component (geographic northward) magnetic disturbance measured by 11 IMAGE stations between 0800 and 1100 UT. The 11 stations are distributed in a north-south chain from NAL at (78.92°N, 11.95°E) to Nurmijarvi (NUR)

at 60.50°N, 24.65°E. The location of NAL is represented in Figure 6c as the asterisk and it can be seen that Cluster-3 was approaching this location during interval C. Starting at 0930 UT, the  $x$  component started to increase steadily at the highest-latitude stations, suggesting a strengthening of the overhead eastward electrojet. There were also  $\sim 12$  min period Pc 5 oscillations throughout the interval, which were coherent with similar oscillations in the  $y$  and  $z$  components (not shown). High-latitude Pc 5 oscillations are often interpreted in terms of active solar wind interactions at the magnetopause, such as the Kelvin-Helmholtz instability, dynamic pressure variations, and flux-transfer events [e.g., *Engebretson et al.*, 1995]. At the time of the sunward burst of convection measured by EDI at 1014 UT, there was a sudden increase in the strength of the Pc 5 oscillations and their period increased to 15–18 min; this pressure change

also marks the start of a sustained period of equatorward migration of the eastward electrojet. The ground-based magnetometer measurements therefore suggest that the burst of sunward convection occurred while Cluster-3 was approaching a region that was coupled to active wave processes in the magnetosphere, possibly generated at the magnetopause. Unfortunately, ground-based auroral imaging data were not available during this period to confirm the existence of discrete auroral arcs on Cluster-3 magnetic field lines. However, measurements from the imaging riometer for ionospheric studies (IRIS) imaging riometer at Kilpisjärvi do show an increase in absorption starting at around 1016 UT (not shown), consistent with enhanced dayside auroral precipitation during this time.

[42] In summary, a sudden sunward burst of convection was measured by EDI during interval C. We postulate that the source of the burst was a sudden decrease in solar wind dynamic pressure that allowed a sunward motion of the dayside magnetopause and a sunward springing of the magnetic field and plasma in the vicinity of all the Cluster spacecraft. Ground-based measurements show that the convection burst occurred while Cluster-3 was approaching magnetic field lines that were coupled to active long-period wave processes, possibly on the magnetopause. At the same time that EDI measured the sunward flow burst in the magnetosphere, an antisunward burst was measured in the ionosphere by SuperDARN. The technique of foot point optimization was unable to reconcile the inconsistency in the SuperDARN and EDI drift directions, suggesting that an electrostatic mapping of electric fields along equipotential magnetic field lines is insufficient during interval C. We therefore conclude that a geophysical explanation for the inconsistency is necessary and postulate that the dominant source is associated with the sudden drop in solar wind dynamic pressure. One element of the magnetospheric response to the pressure decrease would have been a short-lived inductive electric field that would not have mapped to the ionosphere along magnetic field lines. The fact that a small antisunward burst was measured in the ionosphere suggests that some component of the magnetospheric response at high altitude must have been electrostatic. The direction of the burst in the ionosphere may have rotated with respect to the burst at Cluster-3 because of the presence of localized parallel electric fields and/or twisted magnetic flux tubes, also produced by the drop in dynamic pressure.

#### 5.4. Interval D (1100–1145 UT)

[43] During interval D, Cluster-3 was conjugate to the noon-sector convection throat region of the ionosphere, where zonal convection along the morning- and afternoon-sector auroral zones converge and turn northward into the polar cap (see Figure 6d). The spatial coverage of SuperDARN in the vicinity of the Cluster-3 foot point was particularly good during this entire time. Despite this fact, the SuperDARN estimates for the convection at Cluster-3 shown in Figure 7 consistently underestimate the antisunward ( $-X$ ) sense of the flow, while simultaneously over-estimating the dawnward ( $-Y$ ) flow in such a way that the overall strength of the convection is well represented. The procedure of foot point optimization yielded dramatic improvements within 400 km of the nominal T01 foot points, suggesting that the accuracy of

the T01 model might be principally responsible for the inconsistency in this case.

[44] It is interesting to note that the optimized foot points are consistently poleward of the nominal T01 foot points by  $\sim 1^\circ$  in magnetic latitude. In section 4.2, it was shown that the T01 model became increasingly inaccurate in reproducing the FGM measurements during interval D as Cluster-3 approached the dayside magnetopause. This was attributed to the fact that the T01 model does not take account of erosion of magnetic flux from the dayside magnetosphere during extended periods of southward IMF. In particular, it was shown that the T01 model incorrectly estimated a crossing of the open-closed field line boundary during interval D, whereas the FGM measurements suggested that Cluster-3 stayed connected to the open tail lobe throughout. One result of this discrepancy is that Cluster-3 foot points would be shifted poleward of those specified by T01 because the high-altitude ends of open field lines are convected tailward by the solar wind, and hence, would be encountered by Cluster-3 earlier than they would be if they were closed. Erosion of flux from the dayside magnetosphere can thus be invoked to explain the consistent poleward shift of the foot points during interval D. Alternatively, the poleward shift might result from the finite Alfvén transit time between the magnetosphere and the ionosphere. During interval D, Cluster-3 measured strong flows on flux tubes that were convecting into the polar cap with an ionospheric velocity of  $\sim 700$  m/s. A poleward shift of  $\sim 1^\circ$  in latitude is consistent with the distance these flux tubes would travel in a 1–2 min Alfvén transit time from the dayside magnetopause to the ionosphere, a commonly assumed value.

## 6. Summary and Conclusions

[45] A mathematical formalism has been presented that can be used to compare conjugate measurements of plasma convection obtained simultaneously in the magnetosphere and ionosphere. The method relies on the availability of an accurate magnetosphere-ionosphere mapping of magnetic field lines and the assumption that the field lines can be treated as electrostatic equipotentials. To demonstrate the technique we have presented an event study during 0700–1200 UT on 12 March 2001 and compared plasma drift observations from the SuperDARN ionospheric radars with measurements from the EDI experiment on the Cluster-3 spacecraft. The Tsyganenko T01 magnetic field model was used to identify the magnetic foot points of the Cluster-3 spacecraft in the northern ionosphere. During much of the event interval there was good consistency between the EDI and SuperDARN observations. Significant inconsistencies were identified during four subevent intervals labeled A–D and have been explained in terms of one or more of the following influences: (1) localized parallel electric fields; (2) inductive electric fields; and (3) limitations of the T01 model.

[46] In general, the T01 model provided a good representation of the Cluster-3 FGM magnetometer measurements during the event period. However, on the dayside there was evidence that T01 underestimated the magnetic flux in the tail lobe because of an inability to model the cumulative effects of magnetic flux erosion during a sus-

tained period of southward IMF. By searching for improved correspondence between EDI and SuperDARN in locations removed from the nominal foot point location it was demonstrated how conjugate observations can be used to correct small errors in the magnetic mapping. Previous efforts to test the accuracy of magnetic field models have been based on either (1) comparing the model predictions with numerous single-point in situ magnetic field measurements [e.g., Fairfield, 1991; Peredo et al., 1993; Thomsen et al., 1996] or (2) using particle measurements to test the magnetic connectivity between two spacecraft [e.g., Hones et al., 1996; Reeves et al., 1997; Weiss et al., 1997]. The formalism developed in this paper provides a new framework with which to evaluate the performance of magnetic field models and may lead to further model calibrations and refinements.

[47] The most interesting EDI-SuperDARN inconsistencies were identified during intervals A and C when partial decoupling of convection in the magnetosphere and ionosphere was most likely to have occurred. During interval A the Cluster-3 spacecraft was conjugate to the midnight sector auroral zone at a time of increasing geomagnetic activity associated with substorm-like phenomena. During interval C the spacecraft was conjugate to the afternoon-sector polar cap, perhaps close to the open-closed magnetic field line boundary and measured the effects of a sudden drop in solar wind dynamic pressure at the magnetopause. The decoupling of convection during these two intervals can be explained by generation of parallel and/or inductive electric fields associated with dynamic processes in the magnetosphere. If this type of decoupling is a common phenomenon it has serious implications for our ability to monitor magnetospheric dynamics because the cross-polar potential measured at low altitude would not represent the true potential drop across the magnetosphere. This decoupling phenomenon can only be verified by analyzing conjugate observations of electric fields obtained simultaneously in the magnetosphere and ionosphere, as has been presented here.

[48] Future work will expand upon the principles developed in this paper and exploit the full multipoint capability of the Cluster mission. Using MHD models to specify magnetosphere-ionosphere conjugacy, rather than the static T01 model, may improve the identification of inductive electric fields. SuperDARN and EDI measurements will be compared for events during quiet and active conditions in different regions of the magnetosphere. Such a study will provide a quantitative assessment of the occurrence rate of partial decoupled convection throughout the magnetosphere-ionosphere system for different levels of geomagnetic activity.

[49] **Acknowledgments.** Operation of the Northern Hemisphere SuperDARN radars is supported by the national funding agencies of Canada, France, Japan, the United Kingdom, and the United States. Solar wind and IMF data from the ACE spacecraft are courtesy of D. J. McComas and N. Ness. The SYM-H index was obtained from the World Data Center at Kyoto. The IRIS riometer is operated by the Department of Communications Systems at Lancaster University (UK) in collaboration with the Sodankylä Geophysical Observatory and funded by the Particle Physics and Astronomy Research Council (PPARC). We also thank the institutes that maintain the IMAGE magnetometer array and the Canadian Space Agency for providing CANOPUS data. This work was supported by NSF grant ATM-9812078 and NASA grant NAG5-10597. N.A.T. acknowledges

support provided from NSF grant ATM-0296212 and NASA grant NAG5-12185.

[50] Arthur Richmond thanks Stefan Eriksson and Michelle Thomsen for their assistance in evaluating this paper.

## References

- Axford, W. I., and C. O. Hines (1961), A unifying theory of high-latitude geophysical phenomena and geomagnetic storms, *Can. J. Phys.*, **39**, 1443.
- Baker, K. B., and S. Wing (1989), A new magnetic coordinate system for conjugate studies at high latitude, *J. Geophys. Res.*, **94**, 9139.
- Balogh, A., et al. (1997), The Cluster magnetic field investigation, *Space Sci. Rev.*, **79**, 65.
- Baumjohann, W., and G. Haerendel (1985), Magnetospheric convection observed between 0600 and 2100 LT: Solar wind and IMF dependence, *J. Geophys. Res.*, **90**, 6370.
- Block, L. P. (1988), Acceleration of auroral particles by magnetic field-aligned electric fields, *Astrophys. Space Sci.*, **144**, 135–147.
- Boonsirirath, A., R. M. Thorne, G. Lu, V. K. Jordanova, M. F. Thomsen, D. M. Ober, and A. J. Ridley (2001), A semiempirical equatorial mapping of AMIE convection electric potentials (MACEP) for the January 10, 1997, magnetic storm, *J. Geophys. Res.*, **106**, 12,903.
- Boström, R. (1967), Auroral electric fields, in *Aurora and Airglow*, edited by B. M. McCormac, pp. 293–303, Reinhold, New York.
- Bristow, W. A., A. Otto, and D. Lummerzheim (2001), Substorm convection patterns observed by the Super Dual Auroral Radar Network, *J. Geophys. Res.*, **106**, 24,593.
- Doe, R. A., M. B. Moldwin, and M. Mendillo (1992), Plasmopause morphology determined from an empirical ionospheric convection model, *J. Geophys. Res.*, **97**, 1151.
- Donovan, E. F. (1993), Modeling the magnetic effects of field-aligned currents, *J. Geophys. Res.*, **98**, 13,529.
- Donovan, E. F., and G. Rostoker (1991), Internal consistency of the Tsyganenko magnetic field model and the Heppner-Maynard empirical model of the ionospheric electric field distribution, *Geophys. Res. Lett.*, **18**, 1043.
- Dungey, J. W. (1961), Interplanetary magnetic field and the auroral zones, *Phys. Rev. Lett.*, **93**, 47.
- Engelbreton, M. J., W. J. Hughes, J. L. Alford, E. Zesta, L. J. Cahill Jr., R. L. Arnoldy, and G. D. Reeves (1995), Magnetometer array for cusp and cleft studies observations of the spatial extent of broadband ULF magnetic pulsations at cusp/cleft latitudes, *J. Geophys. Res.*, **100**, 19,371.
- Eriksson, S., R. E. Ergun, C. W. Carlson, and W. Peria (2000), The cross-polar potential drop and its correlation to the solar wind, *J. Geophys. Res.*, **105**, 18,639.
- Escoubet, C. P., M. Fehringer, and M. Goldstein (2001), The Cluster mission, *Ann. Geophys.*, **19**, 1197–1200.
- Evans, D. S. (1974), Precipitating electron fluxes formed by a magnetic field-aligned potential difference, *J. Geophys. Res.*, **79**, 2853.
- Fairfield, D. H. (1991), An evaluation of the Tsyganenko magnetic field model, *J. Geophys. Res.*, **96**, 1481.
- Fung, S. F., and R. A. Hoffman (1991), A search for parallel electric fields by observing secondary electrons and photoelectrons in the low-altitude auroral zone, *J. Geophys. Res.*, **96**, 3533.
- Greenwald, R. A., K. B. Baker, R. A. Hutchins, and C. Hanuise (1985), An HF phased-array radar for studying small-scale structure in the high-latitude ionosphere, *Radio Sci.*, **20**, 63.
- Greenwald, R. A., et al. (1995), DARN/SuperDARN: A global view of the dynamics of high-latitude convection, *Space Sci. Rev.*, **71**, 761.
- Gustafsson, G., et al. (1997), The electric field and wave experiment for the Cluster mission, *Space Sci. Rev.*, **79**, 137.
- Heppner, J. P., and N. C. Maynard (1987), Empirical high-latitude electric field models, *J. Geophys. Res.*, **92**, 4467.
- Hesse, M., J. Birn, and R. A. Hoffman (1997), On the mapping of ionospheric convection into the magnetosphere, *J. Geophys. Res.*, **102**, 9543.
- Hones, E. W., M. F. Thomsen, G. D. Reeves, L. A. Weiss, and D. J. McComas (1996), Observational determination of magnetic connectivity of the geosynchronous region of the magnetosphere to the auroral oval, *J. Geophys. Res.*, **101**, 2629.
- Iyemori, T., and D. R. K. Rao (1996), Decay of the *Dst* field of geomagnetic disturbance after substorm onset and its implication to storm-substorm relation, *Ann. Geophys.*, **14**, 608.
- Knight, S. (1973), Parallel electric fields, *Planet. Space Sci.*, **21**, 741.
- Lu, G., M. Brittnacher, G. Parks, and D. Lummerzheim (2000), On the magnetospheric source regions of substorm-related field-aligned currents and auroral precipitation, *J. Geophys. Res.*, **105**, 18,483.
- Maynard, N. C., W. F. Denig, and W. J. Burke (1995), Mapping ionospheric convection patterns to the magnetosphere, *J. Geophys. Res.*, **100**, 1713.
- McComas, D. J., S. J. Blame, P. Barker, W. C. Feldman, J. L. Phillips, P. Riley, and J. W. Griffiee (1998), Solar Wind Electron Proton Alpha

- Monitor (SWEPAM) for the Advanced Composition Explorer, *Space Sci. Rev.*, *86*, 563.
- Mozer, F. S., and C. A. Kletzing (1998), Direct observation of large, quasi-static, parallel electric fields in the auroral acceleration region, *Geophys. Res. Lett.*, *25*, 1629.
- Olsson, A., L. Andersson, A. I. Eriksson, J. Clemmons, R. E. Erlandsson, G. Reeves, T. Hughes, and J. S. Murphree (1998), Freja studies of the current-voltage relation in substorm-related events, *J. Geophys. Res.*, *103*, 4285.
- Paschmann, G., et al. (1997), The electron drift instrument for Cluster, *Space Sci. Rev.*, *79*, 233–269.
- Paschmann, G., et al. (2001), The electron drift instrument on Cluster: Overview of first results, *Ann. Geophys.*, *19*, 1273–1288.
- Pedersen, A., C. A. Cattell, C.-G. Falthammar, V. Formisano, P. A. Lindqvist, F. Mozer, and R. Torbert (1984), Quasi-static electric field measurements with spherical double probes on the GEOS and ISEE satellites, *Space Sci. Rev.*, *37*, 269.
- Peredo, M., D. P. Stern, and N. A. Tsyganenko (1993), Are existing magnetospheric models excessively stretched?, *J. Geophys. Res.*, *98*, 15,343.
- Quinn, J. M., et al. (2001), Cluster EDI convection measurements across the high latitude plasma sheet boundary at midnight, *Ann. Geophys.*, *19*, 1289.
- Reeves, G. D., L. A. Weiss, M. F. Thomsen, and D. J. McComas (1997), A quantitative test of different magnetic field models using conjunctions between DMSP and geosynchronous orbit, in *Radiation Belt Models and Standards*, *Geophys. Monogr. Ser.*, vol. 97, edited by J. F. Lemaire, D. Heynderick, and D. N. Baker, pp. 167–172, AGU, Washington, D. C.
- Reiff, P. H., and J. G. Luhmann (1986), Solar wind control of the polar-cap voltage, in *Solar Wind—Magnetosphere Coupling*, edited by Y. Kamide and J. A. Slavin, pp. 453–476, Terra Sci., Tokyo.
- Richmond, A. D., and Y. Kamide (1988), Mapping electrodynamic features of the high-latitude ionosphere from localized observations: Technique, *J. Geophys. Res.*, *93*, 5741.
- Rino, C. L., V. B. Wickwar, P. M. Banks, S.-I. Akasofu, and E. Rieger (1974), Incoherent-scatter radar observations of westward electric fields, *J. Geophys. Res.*, *79*, 4669.
- Ruohoniemi, J. M., and K. B. Baker (1998), Large-scale imaging of high-latitude convection with Super Dual Auroral Radar Network HF radar observations, *J. Geophys. Res.*, *103*, 20,797–20,811.
- Ruohoniemi, J. M., and R. A. Greenwald (1996), Statistical patterns of high-latitude convection obtained from Goose Bay HF radar observations, *J. Geophys. Res.*, *101*, 21,743.
- Ruohoniemi, J. M., R. A. Greenwald, K. B. Baker, J.-P. Villain, and M. A. McCready (1987), Drift motions of small-scale irregularities in the high-latitude *F* region: An experimental comparison with plasma drift motions, *J. Geophys. Res.*, *92*, 4553.
- Ruohoniemi, J. M., R. J. Barnes, R. A. Greenwald, and S. G. Shepherd (2001), The response of the high-latitude ionosphere to the coronal mass ejection event of April 6, 2000: A practical demonstration of space weather nowcasting with the Super Dual Auroral Radar Network of HF radars, *J. Geophys. Res.*, *106*, 30,085.
- Shepherd, S. G., R. A. Greenwald, and J. M. Ruohoniemi (2002), Cross polar cap potentials measured with the Super Dual Auroral Radar Network during quasi-steady solar wind and interplanetary magnetic field conditions, *J. Geophys. Res.*, *107*(A7), 1094, doi:10.1029/2001JA000152.
- Shue, J.-H., et al. (1998), Magnetopause location under extreme solar wind conditions, *J. Geophys. Res.*, *103*, 17,691.
- Smith, C. W., M. H. Acuna, L. F. Burlaga, J. L. Heures, N. F. Ness, and J. Schiefele (1998), The ACE magnetic field experiment, *Space Sci. Rev.*, *86*, 613.
- Thomsen, M. F., D. J. McComas, G. D. Reeves, and L. A. Weiss (1996), An observational test of the Tsyganenko (T89a) model of the magnetospheric field, *J. Geophys. Res.*, *101*, 24,827.
- Tsyganenko, N. A. (1987), Global quantitative models of the geomagnetic field in the cislunar magnetosphere for different disturbance levels, *Planet. Space Sci.*, *35*, 1347.
- Tsyganenko, N. A. (1989), A magnetospheric magnetic field model with a warped tail current sheet, *Planet. Space Sci.*, *37*, 5.
- Tsyganenko, N. A. (1995), Modeling the Earth's magnetospheric magnetic field confined within a realistic magnetopause, *J. Geophys. Res.*, *100*, 5599.
- Tsyganenko, N. A. (2002a), A model of the near magnetosphere with a dawn-dusk asymmetry: 1. Mathematical structure, *J. Geophys. Res.*, *107*(A7), 1179, doi:10.1029/2001JA000219.
- Tsyganenko, N. A. (2002b), A model of the near magnetosphere with a dawn-dusk asymmetry: 2. Parameterization and fitting to observations, *J. Geophys. Res.*, *107*(A8), 1176, doi:10.1029/2001JA000220.
- Villain, J.-P., G. Caudal, and C. Hanuise (1985), A SAFARI-EISCAT comparison between the velocity of *F* region small-scale irregularities and the ion drift, *J. Geophys. Res.*, *90*, 8433.
- Weimer, D. R. (1995), Models of high-latitude electric potentials derived with a least error fit of spherical harmonic coefficients, *J. Geophys. Res.*, *100*, 19,595.
- Weimer, D. R., J. D. Craven, L. A. Frank, W. B. Hanson, N. C. Maynard, R. A. Hoffman, and J. A. Slavin (1994), Satellite measurements through the center of a substorm surge, *J. Geophys. Res.*, *99*, 23,639.
- Weiss, L. A., M. F. Thomsen, G. D. Reeves, and D. J. McComas (1997), An examination of the Tsyganenko (T89a) field model using a database of two-satellite magnetic conjunctions, *J. Geophys. Res.*, *102*, 4911.
- Wescott, E. M., J. D. Stolarik, and J. P. Heppner (1969), Electric fields in the vicinity of auroral forms from motions of barium vapor releases, *J. Geophys. Res.*, *74*, 3469.
- Yeoman, T. K., J. A. Davies, N. M. Wade, G. Provan, and S. E. Milan (2000), Combined CUTLASS, EISCAT, and ESR observations of ionospheric plasma flows at the onset of an isolated substorm, *Ann. Geophys.*, *18*, 1073.

---

J. B. H. Baker, R. A. Greenwald, and J. M. Ruohoniemi, Applied Physics Laboratory, Johns Hopkins University, 11100 Johns Hopkins Road, Laurel, MD 20723-6099, USA. (joseph.baker@jhuapl.edu)

E. F. Donovan, Department of Physics and Astronomy, University of Calgary, Calgary, Alberta, Canada, AB T2N1N4.

M. Förster and G. Paschmann, Max-Planck-Institut für Extraterrestrische Physik, Postfach 1312, 85741 Garching, Germany.

J. M. Quinn, Department of Physics, University of New Hampshire, DeMerritt Hall, 9 Library Way, Durham, NH 03824-3568, USA.

N. A. Tsyganenko, NASA Goddard Space Flight Center, Code 695, Greenbelt, MD 20771, USA.